Ambiente & Água - An Interdisciplinary Journal of Applied Science
ISSN 1980-993X – doi:10.4136/1980-993X
www.ambi-agua.net
E-mail: ambi.agua@gmail.com

Probabilistic estimation of recharge and its sensitivity to changing precipitation regimes for the Urucuia aquifer, Brazil

ARTICLES doi:10.4136/ambi-agua.3129

Received: 14 Oct. 2025; Accepted: 20 Mar. 2026

Ellen Cristina Oliveira Souza*; Harald Klammler; Luiz Rogério Bastos Leal

Instituto de Geociências. Universidade Federal da Bahia (UFBA), Campus Ondina, Avenida Barão de Jeremoabo, s/n, CEP: 40050-090, Salvador, BA, Brazil. E-mail: hklammler@ufba.br, lrogerio@ufba.br
*Corresponding author. E-mail: ellen.cristina@ufba.br

Editor-in-Chief: Nelson Wellausen Dias

ABSTRACT

Given the rapid expansion of irrigated agriculture and climate change, it is essential to understand the dynamics of groundwater recharge formation for sustainable management of water resources. This study focuses on a portion (≈ 20,000 km^2) of the Urucuia aquifer in northeastern Brazil, for which we use daily hydrometeorological records at five stations over several decades to infer monthly statistics (probabilities and intensities) of precipitation P. We further apply different existing deterministic and probabilistic / stochastic soil water balance approaches to estimate recharge R for the past and a limited number of possible future scenarios. Long-term average recharge estimates range from 257 to 440 mm/year (east to west) with recharge events concentrated exclusively in the rainy summer months. For annual averages in mm/day, we identify the empirical relationship $R = P - 2$ as a simple and accurate approximation for the region. We further conclude that quantification of recharge as a percentage of precipitation is inappropriate and that seasonal variability with soil water carry-over between seasons cannot be neglected. Future scenarios with reduced average precipitation are estimated to affect groundwater recharge over-proportionally and stronger than soil water content.

Keywords: climate change, evapotranspiration, groundwater, soil water balance, stochastic simulation.

Estimativa probabilística da recarga e sua sensibilidade a mudanças nos regimes de precipitação para o aquífero Urucuia, Brasil

RESUMO

Diante do crescente avanço da agricultura irrigada e das mudanças climáticas, torna-se essencial compreender a dinâmica da recarga de águas subterrâneas para a gestão sustentável dos recursos hídricos. Este estudo foca em uma porção (≈ 20.000 km^2) do aquífero Urucuia no nordeste do Brasil, para qual são utilizados dados hidrometeorológicos diários de cinco estações durante várias décadas, a fim de inferir estatísticas mensais (probabilidades e intensidades) de precipitação P. Foram aplicadas diferentes abordagens existentes de balanço hídrico do solo, tanto determinísticas quanto probabilísticas / estocásticas, para estimar a recarga R em cenários passados e em um número limitado de cenários futuros possíveis. As estimativas de recarga média de longo prazo variam de 257 a 440 mm/ano (de leste para oeste), com eventos de recarga concentrados exclusivamente nos meses chuvosos de verão. Para médias anuais em mm/dia, é identificada a relação empírica $R = P - 2$ como estimativa simples e precisa para a região. É concluído ainda que quantificar a recarga como uma porcentagem da precipitação é inadequado, e que a variabilidade sazonal com transferência de umidade do solo entre estações não pode ser negligenciada. Cenários futuros com redução de precipitação média devem afetar a recarga de água subterrânea de forma mais acentuada que o conteúdo de umidade do solo.

Palavras-chave: águas subterrâneas, balanço hídrico do solo, evapotranspiração, mudança climática, simulação estocástica.

1. INTRODUCTION

Groundwater is essential for supporting economic activities, supplying urban and rural areas, and sustaining aquatic ecosystems such as rivers, lakes, mangroves, and wetlands. It represents 97% of the planet's freshwater, making aquifers the largest reservoir of potable water available to humanity (Hirata *et al.*, 2019). In western Bahia, the Urucuia Aquifer System (UAS) represents a strategic resource, mainly due to its significant contribution to maintaining baseflows of the São Francisco River's tributaries, and due to the increasing water demand associated with the considerable expansion of agricultural activity since the 1980s (Gaspar, 2006; Oliveira *et al.*, 2019).

Located in the MATOPIBA frontier, the portion of the UAS situated in western Bahia faces various pressures on its water system, particularly due to the implementation of large irrigation projects using center pivots for soybean and cotton cultivation. This raises concerns about water quality and the reduction of water volumes in the water bodies (ANA, 2017; Oliveira, 2021). The MATOPIBA areas feature key conditions for modern industrial agriculture, such as flat terrain, productive soil, and favorable climate, highlighting the region's potential in arable land and establishing it as a new frontier for agricultural expansion in Brazil (Brasil, 2018; Miranda *et al.*, 2014; Polizel *et al.*, 2021).

Conflicts related to water use in western Bahia reflect the growing dispute over water resources between local communities and large agricultural enterprises. Since the mid-2010s, a significant reduction in river flow volumes has been observed, which has raised questions regarding the granting of water-use permits and the effectiveness of hydrological monitoring in the region. The most emblematic episode occurred in 2017, when around two thousand people invaded the Igarashi farm in Correntina to protest against the excessive water withdrawal for irrigation. These events highlight the increasing tensions resulting from the expansion of agribusiness (Coelho, 2024).

Although often attributed to the expansion of irrigation systems, the conflicts in the region are also significantly influenced by natural factors, particularly climatic variability. Its geographic location, in a transitional zone between semi-arid tropical and seasonally dry climates, makes the area particularly vulnerable to the effects of climate change (Pousa *et al.*, 2019). Moreover, the UAS recharge area consists of the predominant high-plain regions, which have already been affected by anthropogenic impacts altering infiltration / recharge conditions, besides the risk of groundwater overexploitation by high irrigation demands in the region (ANA, 2017; Gaspar and Campos, 2007). Therefore, assessing the potential impacts of climate change and human impacts on water resources is essential, given their broad implications.

In this context, estimating groundwater recharge is a key prerequisite for planning and managing water resources, especially in regions that rely on these resources for irrigated agricultural activities (Eilers, 2004). In certain aquifers, the deficit between natural recharge and water demand already requires unconventional interventions to ensure water supply (Al-

Najjar *et al.*, 2021). Projections based on Global Climate Models indicate a trend toward decreasing precipitation and increasing temperatures, which may intensify pressure on aquifers and lead to a significant decline in groundwater levels over the coming decades (Al-Najjar *et al.*, 2022). Such examples further reiterate the need for robust modeling approaches to mitigate long-term water stress.

Estimating recharge remains a significant challenge, as there is no universally accepted methodology for its quantification (Scanlon *et al.*, 2002). Rainfall infiltration and water balance approaches have been highlighted for their simplicity and effectiveness in estimating groundwater recharge (Kumar *et al.*, 2022). Pontes *et al.* (2016) state that among the various ways to estimate recharge, the soil zone water balance is the simplest, as it requires few data inputs. Several methods are used to model the water balance in the soil zone, including mathematical approaches such as Balseq (Lobo-Ferreira *et al.*, 2014) and Thornthwaite-Mather (Thornthwaite, 1948; Thornthwaite and Mather, 1955), and computational models like Hydrobal (Touhami *et al.*, 2014). Most models incorporate land use and land cover and are adaptable to different scales, in addition to being useful for predicting soil moisture and vegetation water stress.

In addition to soil water balance models, alternative techniques have been employed to assess the dynamics of groundwater resources. Among these, techniques that use time-variable gravity data stand out, such as those obtained from the Gravity Recovery and Climate Experiment (GRACE) mission, which have become important tools for monitoring variations in water mass. This geophysical remote-sensing technology enables a broader understanding of changes in water storage and aquifer dynamics under different hydrological regimes and anthropogenic pressures (Othman *et al.*, 2022).

Another widely used approach for estimating recharge is based on the direct observation of water table fluctuations in wells, which is known for its simplicity, low cost, and ability to provide quick and practical estimates. The technique is based on analyzing the water table dynamics with a known or estimated value of specific yield. However, compared to other recharge estimation methods, this method tends to overestimate values, as it considers water table fluctuations that are not always exclusively related to recharge (Becke *et al.*, 2024). Due to the relatively deep (up to 100 m) water table under the Urucuia high-plains and the significant effect of the unsaturated zone on recharge propagation, this method is not deemed appropriate for the present study.

Groundwater recharge is also expected to be highly susceptible to the impacts of climate change. Adhikari *et al.* (2022) highlighted the importance of investigating these effects for efficient planning and sustainable water resource management. Although the methods used in this type of analysis have advanced, their application in decision-making remains limited due to associated uncertainties. Probabilistically quantifying the confidence level in future recharge projections can help managers define more assertive strategies. However, such studies present challenges, since groundwater responds differently to climate variations than surface water. Gebru *et al.* (2024) conducted a review of the main methods used to estimate groundwater recharge in Ethiopia, identifying major limitations such as a lack of accurate data and the absence of adequate validation of results, which compromises the reliability of estimates. The authors also stress the need to consider the impacts of climate change to assess the long-term effects on groundwater recharge.

The IPCC (2022) report projects a reduction in rainfall in northern South America, with an increase in consecutive dry days and historically unprecedented droughts in the region. Additionally, an increase in evapotranspiration has been observed since the 1980s, along with a reduction in soil moisture across arid, humid, and transitional regions. In a simulation projecting future recharge (2041–2060) for the UAS in an optimistic scenario, Pereira (2021) concluded that recharge could decrease by up to 27%, whereas in a pessimistic scenario, the reduction could reach up to 43%.

The objectives of this study are to characterize the seasonal (i.e., monthly) statistics of precipitation and to assess the recharge R in a portion of the UAS corresponding to the Corrente River basin. The latter is achieved by using the soil water balance framework of Porporato *et al.* (2004) with extensions for seasonal variations by Feng *et al.* (2015). In particular, three approaches are applied and compared: (1) direct deterministic simulation with existing time series of precipitation P and potential evapotranspiration PET (Section 2.2) for calibration of soil water capacity; (2) probabilistic estimation using existing analytical solutions and statistics of P (with and without seasonal carry-over of soil water between months; Section 2.3); and (3) stochastic Monte Carlo simulation with future projections of seasonal P statistics (Section 2.4). For a comprehensive flowchart of the methodological approach and article structure, see Figure 1. The simulation results are used to infer a very simple and practical relationship between the annual means of precipitation and recharge. Overall, this study provides fundamental mechanistic insight on recharge formation at the daily and seasonal time scales in the soil zone of the Urucuia aquifer, which is limited, however, to simplified natural conditions not including areas of (partially irrigated) agriculture in the region.

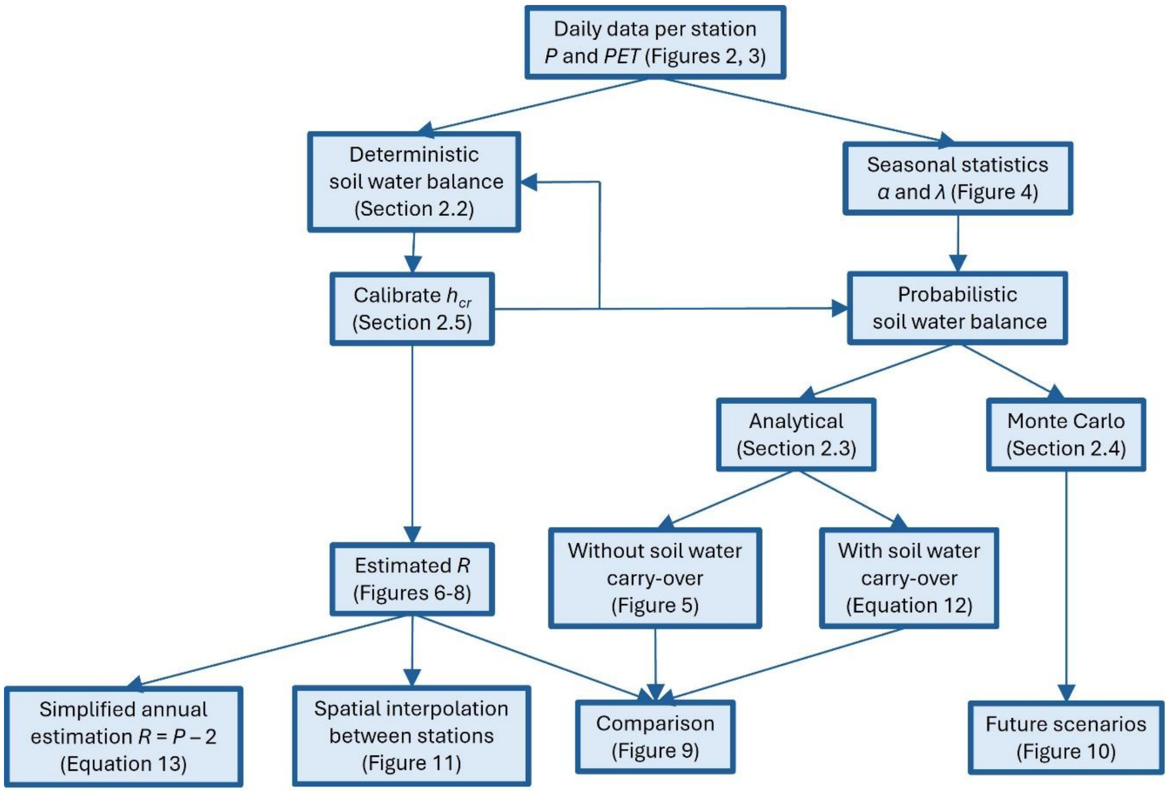

Figure 1. Flowchart representing the methodological approach and article structure.

2. MATERIAL AND METHODS

2.1. Study Area

The study focuses on the central-western portion of the Corrente River basin (Figure 2), partially covering the municipalities of Correntina, Cocos, Coribe, and Jaborandi. The area of approximately 18,000 km² encompasses the sub-basins of the Éguas, Arrojado, and Formoso rivers. The region is mainly characterized by a flat-topped plateau (high-plain), with altitudes ranging from 470 to 1,016 meters over approximately 200 km from east to west, and predominantly parallel to subparallel drainage patterns (Oliveira *et al.*, 2020). The northern, western, and southern boundaries are defined based on topographic highs, while the eastern boundary was determined by the area containing the Correntina, Arrojado, and Gatos hydrometeorological stations.

The geological units occurring in the study area belong to the Urucuia Group and can reach thicknesses of up to 400 meters. These highly homogeneous units overlie a basement of Proterozoic rocks and generally present high textural and mineralogical maturity. From this perspective, the UAS consists of a set of interconnected aquifers developed in sandstones with relatively high effective porosity. Although spatially limited silicified sandstone levels may exist, the UAS as a whole presents unconfined conditions with a free groundwater table receiving recharge through the overlying unsaturated zone (Barbosa *et al.*, 2017).

The Posse Formation, the basal unit of the Urucuia Group, is composed of fine to medium sandstones that indicate an aeolian depositional environment with characteristics of dune fields and interbedded fluvial processes. Above it is the Serra das Araras Formation, which is distinguished by its greater lithological diversity. Composed mainly of sandstones, this formation is characterized by a balanced depositional environment between aeolian and fluvial processes, and it is thicker and more extensive than the Posse Formation (Campos and Dardenne, 1997; ANA, 2017). Soils are derived from the spatially very uniform sandstone and also correspondingly homogeneous of sandy latosol and quartzarenic neosol types (Gaspar *et al.*, 2007).

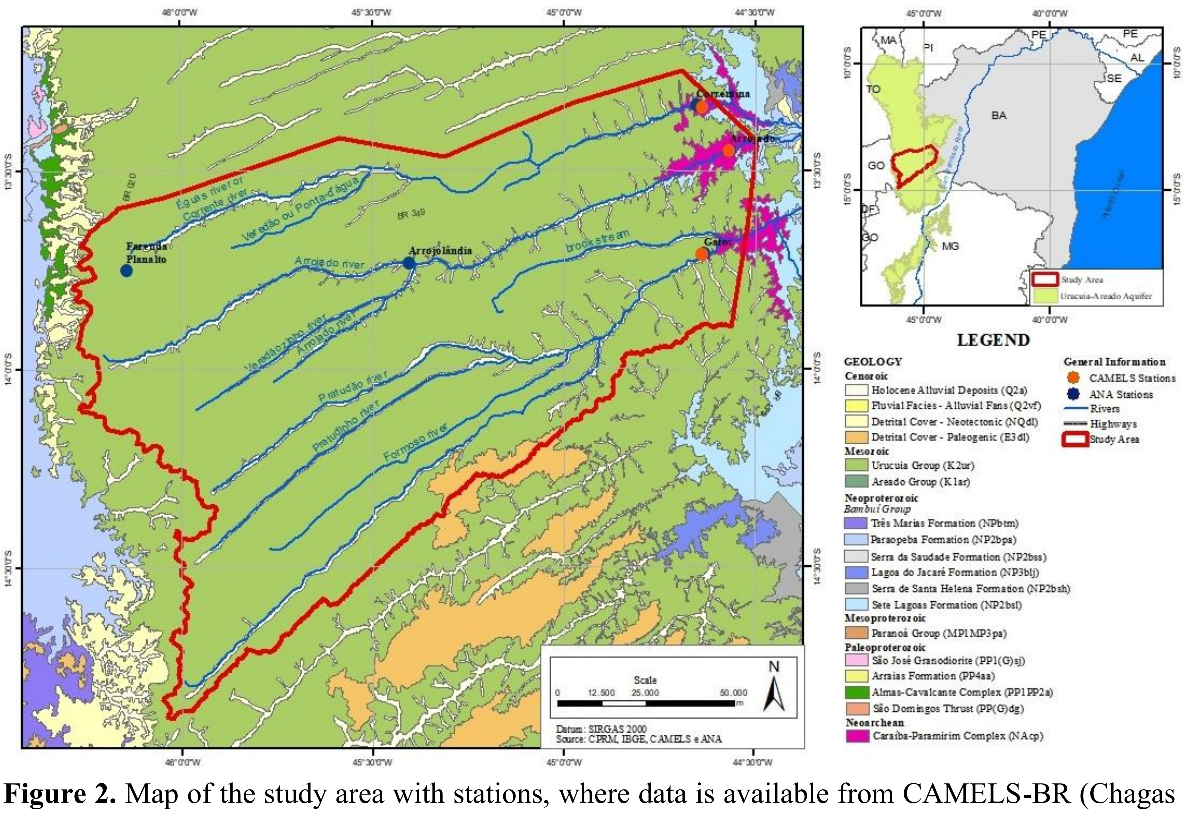

Figure 2. Map of the study area with stations, where data is available from CAMELS-BR (Chagas *et al.*, 2020) or ANA (2024), showing also the main rivers and predominant geology of the Urucuia Group. Other rain gauge stations exist within the study area but were excluded due to very short or incomplete records and / or a significant amount of inconsistent data (outliers).

Land use in the study area is characterized by a strong presence of agriculture, with emphasis on both large-scale and small-scale irrigated farming, in addition to pastures, native vegetation of the Cerrado biome, urban areas, and water bodies (Mantovani *et al.*, 2019). According to Köppen's classification, the climate in the study area is tropical with a dry winter (type Aw), presenting a temperature range between 20°C and 26°C. This climate is marked by strong seasonality and high evapotranspiration during the wet summer months (Figure 3). In the long term, average potential evapotranspiration *PET* is approximately 3 mm/day, while average precipitation *P* varies from 1.5 to 3 mm/day mainly from east to west (Oliveira *et al.*, 2020).

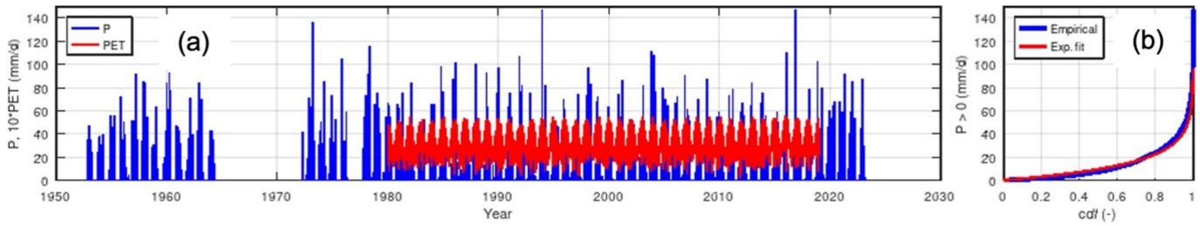

Figure 3. Example of available climate data. (a) Daily time series of precipitation *P* at the Gatos station (ANA, 2024); for other stations, see Supplemental Material) and potential evapotranspiration *PET* (Chagas *et al.*, 2020; 10 times exaggerated relative to *P*) in the study area, showing strong seasonality with dry winters and rainfall concentrated in the summer during periods of high *PET*. Since *PET* is very uniform across the study area (high correlation among the Gatos, Arrojado, and Correntina stations) and data are unavailable for the other stations investigated, we used the average *PET* from these three stations for the entire area. (b) Cumulative distribution (cdf) of daily rainfall on rainy days (i.e., excluding dry days) with a fitted exponential distribution (as used by Porporato *et al.*, 2004), showing good agreement.

2.2. Daily Soil Water Balance

We conduct a regional-scale recharge study using the daily soil water balance over time t [T] (Porporato *et al.*, 2004). The "soil" is considered as the rooting zone of vegetation with a depth Z [L] and a relative moisture content w [-], defined as the volume of water per total soil volume. Soil moisture w can vary between a minimum residual value w_{res} [-] and a maximum critical value w_{cr} [-]. The absolute volume of water in the soil per unit surface area is therefore equal to wZ. The soil gains water from precipitation P [LT^{-1}] and loses water through evapotranspiration ET [LT^{-1}] and deep percolation R [LT^{-1}], interpreted as recharge (usually at the top of the unsaturated zone) to the aquifer, since surface runoff is negligible in the study area. For $w = w_{res}$, the soil is dry and ET becomes zero; near $w = w_{cr}$, the soil is close to field capacity, and ET reaches its maximum as potential evapotranspiration PET [LT^{-1}] for a given day. For intermediate values of w, the model assumes a linear relationship between the two limits, expressed as Equation 1:

$$ET = \frac{w - w_{res}}{w_{cr} - w_{res}} PET \tag{1}$$

The corresponding soil water balance is Equation 2:

$$Z\frac{dw}{dt} = P - ET - R \tag{2}$$

where daily values of R are calculated to keep $w \leq w_{cr}$ for given time series of P and PET. In other words, on days when w would exceed w_{cr}, recharge R is exactly the amount of water that drains from the soil downward to bring w back to w_{cr}. During prolonged dry periods with $P = 0$, w approaches w_{res}, causing ET to approach zero, and the soil remains in a stable dry state.

Multiplying both the numerator and denominator of Equation 1 by Z and introducing $h = Z(w - w_{res})$ and $h_{cr} = Z(w_{cr} - w_{res})$ [L] as the dynamic and critical water volumes in the soil per unit surface area, we can simplify Equation 1 to Equation 3:

$$ET = \frac{h}{h_{cr}} PET \tag{3}$$

This shows that the three soil-specific parameters Z, w_{res}, and w_{cr} can be summarized in a single value h_{cr}, which is needed to partition P into ET and R. We also note that $Z\,dw/dt$ in Equation 2 directly corresponds to dh/dt, leading to the water balance in terms of h as in Equation 4.

$$\frac{dh}{dt} = P - \frac{h}{h_{cr}} PET - R \tag{4}$$

Using the finite difference method for day i [-] with Δt = 1 day and $\Delta h = h_{i+1} - h_i$, we implemented Equation 4 numerically as Equation 5.

$$h_{i+1} = h_i + \left(P_i - \frac{h_i}{h_{cr}} PET_i - R_i\right)\Delta t \tag{5}$$

where the time series of R_i results to keep $h \leq h_{cr}$, i.e., $R_i = h_i - h_{cr}$ on days when $h_i > h_{cr}$, while $R_i = 0$ at other times. This implementation can be automated using software such as Excel or GNU Octave 8.2.0, as done in this study.

2.3. Probabilistic Soil Water Balance

To assess the effects of climate change, for example, the water balance from Section 2.2 has been extensively studied, including probabilistic aspects related to ecosystem responses (Porporato *et al.*, 2004) and streamflow in watersheds (Botter *et al.*, 2007). In this framework, PET is considered constant, and stochasticity is introduced through random precipitation P with a daily probability λ [1/d] and a mean intensity α [mm] on days when $P > 0$ (i.e., excluding dry days with $P = 0$). Both λ and α are also considered constant, resulting in a constant average precipitation $\langle P\rangle = \lambda\alpha$. This approach also assumes that days with precipitation follow a random sequence over time (Poisson distributed), while daily precipitation intensities follow an exponential distribution (Figure 3b and Supplemental Material for stations studied here containing seasonality), which is widely verified in practice (Porporato *et al.*, 2004).

Based on this, advanced mathematical operations yield an estimate of the average $\langle h\rangle$ of the water available in the soil as given by Equation 6 (Porporato *et al.*, 2004, their Equations 3 and 4):

$$\frac{\langle h\rangle}{h_{cr}} = \frac{1}{\phi} - \frac{A^{\frac{A}{\phi}-1}}{\gamma(\frac{A}{\phi},A)} e^{-A} \tag{6}$$

where the aridity index is defined by Equation 7:

$$\phi = \frac{PET}{\langle P\rangle} \tag{7}$$

and the normalized soil water storage capacity by Equation 8:

$$A = \frac{h_{cr}}{\alpha} \tag{8}$$

Both are dimensionless constants, while $\gamma(A/\phi, A)$ is the lower incomplete gamma function of A/ϕ from zero to A. Using Equation 3, this implies an average $\langle ET\rangle$ for actual evapotranspiration as given by Equation 9:

$$\langle ET\rangle = \frac{\langle h\rangle}{h_{cr}} PET \tag{9}$$

and, from Equation 4 with $dh/dt = 0$ (steady-state water balance), it also yields the average recharge $\langle R\rangle$ as estimated in Equation 10:

$$\langle R\rangle = \langle P\rangle - \langle ET\rangle \tag{10}$$

Given meteorological data (precipitation statistics λ and α, and a *PET* value) and soil / vegetation characteristics (porosity, residual and critical moisture, and rooting depth, all summarized in parameter h_{cr}) for a region, Equations 6 to 10 provide a direct estimate of the probabilistically expected recharge rate $\langle R\rangle$. Consequently, these equations also make it easy to quantify the sensitivity of $\langle R\rangle$ to variations in input parameters for assessing future climate or land use / vegetation change scenarios. The most complex part of this process is computing the gamma function in Equation 6, which can be handled with Excel or GNU Octave 8.2.0, as in this work.

Combining Equations 6, 9, and 10, the expected recharge can be expressed as a proportion of average precipitation by Equation 11:

$$\frac{\langle R\rangle}{\langle P\rangle} = \phi \frac{A^{\frac{A}{\phi}-1}}{\gamma(\frac{A}{\phi},A)} e^{-A} \tag{11}$$

As expected, and despite the multiplication by aridity index ϕ in Equation 11, recharge decreases with growing ϕ (i.e., more energy for *ET* and less available *P*) and with higher values of *A* (i.e., greater soil water storage increases *ET* availability).

For variable climates (e.g., seasonal), these results only hold for soils with low water storage capacity, so that the soil moisture state rapidly adjusts (on a daily scale) to new climate conditions. Here, we apply the truncated gamma distribution approximation (Feng *et al.*, 2015) to better account for the seasonal variations of *PET* and especially λ and α in the study area. Based on the water balance in Equation 4 and monthly $\langle h\rangle$ estimates from Equation 6, this approximation becomes Equation 12:

$$\frac{d\langle h_t\rangle}{dt} = \alpha_t\lambda_t - \frac{\langle h_t\rangle}{h_{cr}} PET_t - \langle R_t\rangle \tag{12}$$

where we add the subscript "*t*" to indicate time dependence. The adjusted recharge $\langle R_t\rangle$ is obtained from Equation 11 using a value of λ (embedded in ϕ) so that $\langle h\rangle = \langle h_t\rangle$ in Equation 6. As in Equation 5, Equation 12 is implemented using the finite difference method with time steps $\Delta t = 1$ day. Since the forcing variables α_t, λ_t, and PET_t are annually periodic, the numerical simulation ends when periodic stability is achieved within a small tolerance margin.

2.4. Stochastic Simulation (Monte Carlo)

The Monte Carlo simulation consists of numerically modeling a deterministic process repeatedly, for example, with random input parameters and / or data within their probabilistic characteristics. Although it requires greater computational effort, this method combines the advantages of Sections 2.2 and 2.3, allowing Equation 5 to be applied with synthetic rainfall time series generated using variable λ and α parameters throughout the year due to climatic seasonality. Based on the resulting simulations of h_i, ET_i, and R_i, it is possible to estimate averages and ranges of variability for each day or month of the year, while PET_i may also vary over time and / or include uncertainty. This enables future projections not only in terms of expected values (as in Section 2.3), but also accounting for associated uncertainties. Moreover, it is applicable in scenarios involving seasonal climate variation and considerable soil water storage capacity (Feng *et al.*, 2015).

Since available *PET* data do not cover the same periods as the rainfall data, and given the high consistency in *PET*'s seasonal variability across different years (Figure 3a), we used average monthly *PET* values (Figure 4) for all years. This also allows the simulation of future scenarios with different rainfall parameters. We considered four scenarios, always in comparison to the baseline scenario (Figure 4), as follows: (1) 10% reduction in α with λ unchanged, (2) 10% reduction in λ with α unchanged, (3) simultaneous 10% reduction in α and 10% increase in λ, and (4) simultaneous 10% reduction in λ and 10% increase in α. While average rainfall in scenarios (1) and (2) also decreases by 10%, it remains unchanged in scenarios (3) and (4). Simulations with exponentially distributed rainfall heights (Figure 3b) were generated for 100 years with an additional year at the beginning, which was disregarded in the results to avoid model initialization effects.

2.5. Parameter Definition

The single model parameter to be defined is the critical soil water storage h_{cr} in Equation 4, which affects the timing and average amount of groundwater recharge *R* generated by the soil zone. Higher values of h_{cr} allow for larger soil water storage, thus making more water available for *ET* and reducing *R*, while lower values of h_{cr} achieve the opposite effect. Over the long term when changes in storage can be neglected, averages of *R* have to correspond to averages of river discharge *Q* per unit catchment area, given that direct surface runoff (overland flow to rivers) is virtually non-existent in the study region. Based on this, h_{cr} = 250 mm is adopted here, generating a long-term average recharge estimate of 352 mm/year for the Gatos station. This compares well with observed values of 342 and 366 mm/year for the full historical period of record and before 1980 only, when both potential reductions of river discharge due to extensive groundwater pumping as well as vegetation and soil use changes due to (partially irrigated) agriculture may still be neglected.

Given a soil porosity of approximately 30% in the region (Mantovani *et al.*, 2019), residual and critical saturation values of 0.1 and 0.3 correspond to w_{res} = 0.03 and w_{cr} = 0.09, respectively. The Cerrado biome is characterized by a wide diversity of plant species, with rooting systems ranging from shallow to deep and species adaptation to drought periods (Rawitscher *et al.*, 1943; Canadell *et al.*, 1996). Oliveira *et al.* (2005) observed that, in the "campo sujo" physiognomy, which is predominant in the study area especially prior to 1980, roots reached depths of up to 4 m. Thus, adopting a rooting depth of Z = 4 m also results in a critical soil water capacity $h_{cr} = Z(w_{cr} - w_{res}) \approx 250$ mm, which suggests that the calibrated value is not only consistent with observed river discharge, but also with regard to regional soil and vegetation conditions.

3. RESULTS

The statistical analysis of the hydrometeorological data from the Gatos station between 1953 and 2023 (Figure 3a) reveals the overall seasonal characteristics in the monthly averages of precipitation *P* and potential evapotranspiration *PET* (Figure 4). Monthly *PET* ranges between 2 and 4 mm/day and presents a significantly weaker seasonality than *P*, which varies from 0 to 8 mm/day. After maximum values in November and December, a smooth decline in *P* is observed in January and February, followed by a sharp drop to near-zero values from May through September. The daily precipitation probability λ and its intensity α follow a similar pattern showing that the rainy season is marked by both more frequent and stronger precipitation events. During the wettest time of the year in November and December, there is an almost 50% chance of rain per day with average amounts of approximately 16 mm/day.

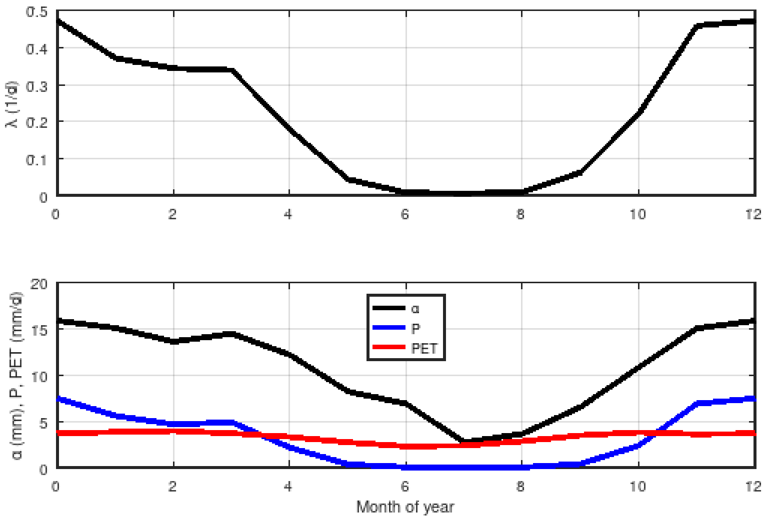

Figure 4. Monthly average climate parameters for the Gatos station inferred from data in Figure 3a. (a) Daily probability λ of rainfall, and (b) average rainfall height α on rainy days, along with monthly averages of precipitation P and potential evapotranspiration PET.

A graphical analysis of Equation 11 is in agreement with expectation that as the aridity index Φ increases, the expected recharge as proportion of precipitation tends to decrease (Figure 5). It is also observed that greater soil water storage capacities with larger values of A (Equation 8) result in reduced recharge, since more water is available to be extracted via ET. Moreover, the larger A, the steeper and larger is the drop in recharge with Φ, potentially reaching zero. While A at the Gatos station (red circles) varies between approximately 15 and 80, the graph for A = 20 (dark brown line) appears to be an accurate approximation for all months. Such a high value of A indicates that soil water storage capacity is much larger than expected rainfall intensity, making isolated precipitation events highly unlikely to generate groundwater recharge. Instead, recharge may be triggered more easily during the rainy season, when repeated rainfall fills up the soil water storage for subsequent precipitation events to surpass the critical level. As a further consequence, the portion of precipitation becoming recharge is more sensitive to Φ than A, which is illustrated by a clear reduction in relative recharge from almost 60% at Φ = 0.5 to zero for values above 1.5.

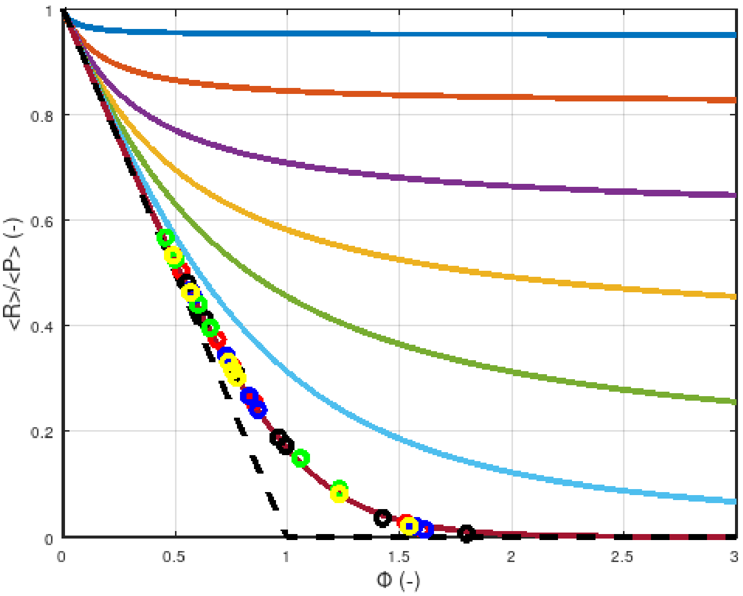

Figure 5. Representation of Equation 11 for different values of A = {0.05, 0.2, 0.5, 1, 2, 5, 20} (solid colored lines from top to bottom), indicating the wettest months (circles) at the Gatos (red), Arrojado (blue), Correntina (black), Fazenda Planalto (green), and Arrojolândia (yellow) stations for h_{cr} = 250 mm. The dashed black line corresponds to $A \rightarrow \infty$, i.e., very large soil water storage capacities, where <*R*> = <*P*> - PET for <*P*> > PET (energy-limited *ET*), and <R> = 0 otherwise (water-limited *ET*). All data cluster around the A = 20 line (Equation 8). Months not shown in this figure have $P \approx 0$, thus lying outside the chart with very high Φ and $R \approx 0$.

The results from the daily soil water balance modeling of Equation 5 (Figure 6 with zoom in Figure 7) are based on constant monthly values of *PET* (Figure 4b). This is justified by the relatively uniform annual cyclicity of *PET* and allows for executing the simulation including periods where data for *P* are available, while those for *PET* are not (Figure 3a). The long-term averages of observed *P* and simulated recharge *R* amount to 1064 and 352 mm/year (approximately 33% of *P*), respectively. Moreover, there are consistent seasonal patterns among *P*, *ET*, *h* and *R* over time. Variability in *ET* aligns strongly with the soil moisture *h* due to the relatively small variability in *PET*. Recharge *R* is marked by peaks during the two to three months with greatest precipitation. However, the first precipitation events of a rainy season do not generate recharge, but increase the soil water content for subsequent rainfall to trigger recharge events, when $h > h_{cr}$. These results highlight the dominant influence of *P* on both *ET* and *R*, through their relationship with soil water availability *h*.

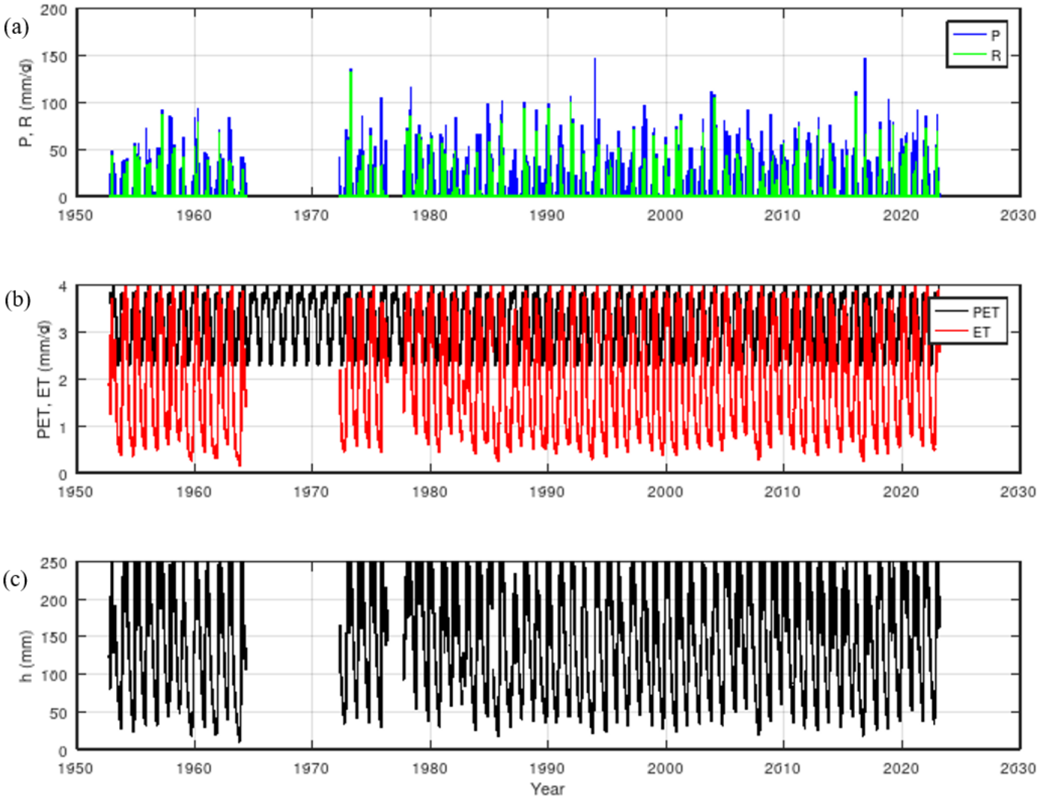

Figure 6. Simulation of the historical daily soil water balance at Gatos based on Equation 5 in terms of (a) precipitation P and recharge R, (b) potential evapotranspiration PET and actual evapotranspiration ET, and (c) soil water content h. The long-term averages of P and simulated R are 1064 and 352 mm/year, respectively.

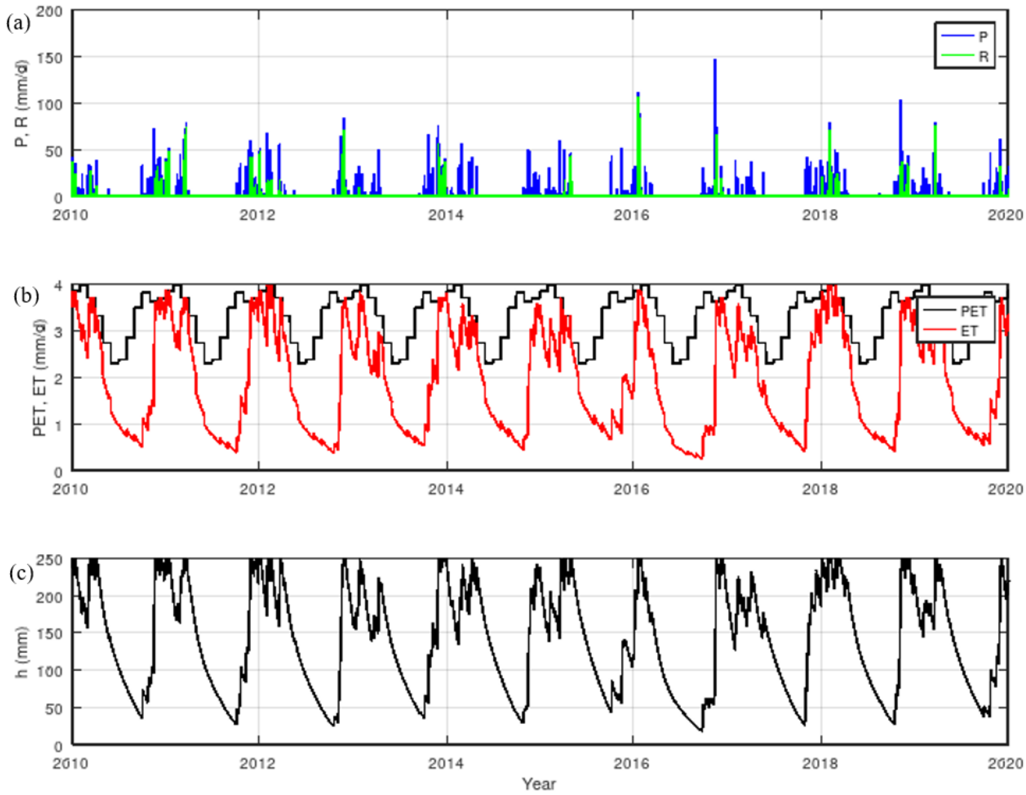

Figure 7. Zoom into Figure 6 for the 10-year interval from 2010 to 2020.

Based on the daily simulation results of Figure 6, we compute annual averages of *P*, *ET* and *R* for a direct comparison (Figure 8). The averages are taken from July of one year to June of the subsequent year, such that the transitions coincide with the dry season of the year and soil water content h is consistently on the well-defined falling limb near 100 mm (e.g., Figure 7). For a negligible variation in h at the transition points in each year, the annual soil water balance simplifies to $R = P - ET$, and more specifically to the approximate relationship of Equation 13.

$$R \approx \begin{cases} P - 2 & for \quad P \geq 2 \\ 0 & for \quad P < 2 \end{cases} \tag{13}$$

with *R* and *P* in mm/day. This is inferred from Figure 8 (red line) demonstrating that $ET \approx 2$ mm/day is a highly accurate (±10%) approximation. The second condition is included to avoid negative values of *R*, which would correspond to a consumption of groundwater from the saturated zone by *ET*. Due to the generally deep water tables, this is unreasonable for our field sites, while also consistent with the modeling approach in Section 2.2. The approximate estimates of annual *R* from Equation 13 (black line) agree well with full simulation results (green line). This demonstrates that the emerging behavior of annual *ET* being highly constant near 2 mm/day observed from the daily soil water balance simulation allows for this very simple and practical annual recharge estimation method based on annual data of *P* only. Notably, the relationship of *R* is not a fraction (percentage) of *P*, but rather an excess quantity with respect to a constant threshold.

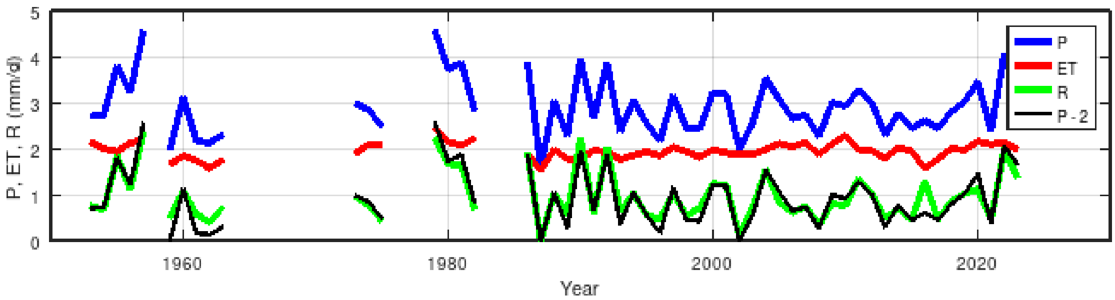

Figure 8. Annual averages from July to June corresponding to simulation results of Figure 6 with gaps due to missing data values in observed *P* time series. Actual evapotranspiration *ET* remains consistently close to 2 mm/day, suggesting the very simple and practical relationship $R \approx P - 2$ with $R \geq 0$ (black line; Equation 13) for annual averages of R (green line) in mm/day.

Besides annual averages, the simulated model results may also be represented in terms of averages for each month of the year (Figure 9, bold continuous lines labeled "Simulation continuous") with corresponding 90% ranges of variability (thin dotted lines labeled "Range (90%)"). Recharge is seen to occur exclusively in the months from November to April with large ranges of variability bounded by zero from below. This means that although recharge is concentrated in this season, there is still a chance that it is zero in one or more of these months, or much larger than the average. From May to October recharge is rigorously zero without any variability at all. In a similar fashion, *ET* and h present seasonal variabilities peaking in the summer, however, with smaller variability ranges and not reaching zero in the winter months, which is important from an ecological / vegetation perspective.

The representation of Figure 9 also allows for a direct comparison to the analytical estimates of Section 2.3., which we call "Analytical by month" (hereafter AM; Equations 6, 9 and 10) and "Analytical continuous" (hereafter AC; Equations 6, 9 and 10 with Equation 12 for soil water carry-over between months). For recharge, both AM and AC agree well with the full simulation results, except for the month of November, where AM significantly overestimates.

This is due to the fact that this method ignores the very low soil moisture content of the preceding months (black line), such that precipitation erroneously starts triggering recharge, instead of first filling up soil water storage. On the other hand, there is a small but consistent underestimation for the months from January to April, which over the whole year contributes to an only slightly larger recharge estimate of 379 mm/year.

In terms of *h* and *ET*, the AM approach clearly underestimates during the dry season, which is again because carry-over of soil water from previous months is not accounted for. For these reasons, the AM approach is found to be inappropriate for the study area. In contrast, the AC method remediates exactly this deficiency and achieves significantly improved estimates of *R*, *ET* and *h* throughout the year with a smaller annual recharge estimate of 290 mm/year, however. This underestimation with respect to the simulation is small (and clearly within the 90% variability bounds) but consistent over the months and may be due to deviations from the analytical model assumptions (e.g., deviations of the historical data from the assumptions of Poisson distributed precipitation days and exponentially distributed precipitation intensities).

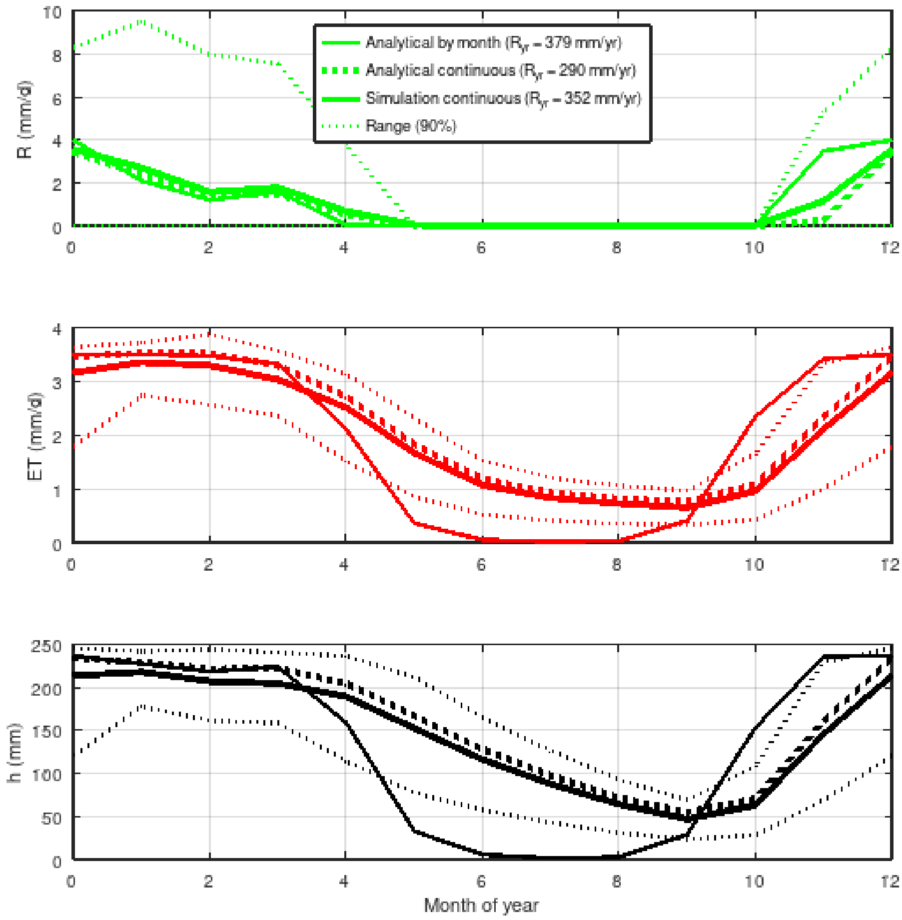

Figure 9. Comparison of estimates for recharge *R* (green), actual evapotranspiration *ET* (red), and soil moisture *h* (black) from different modeling approaches. "Analytical by month" uses monthly averages of Figure 4 for evaluation of Equations 6, 9 and 10 separately for each month of the year (without soil water carry-over between months; Porporato *et al.*, 2004). "Analytical continuous" is like "Analytical by month", but with inclusion of Equation 12 to account for soil water carry-over between months (Feng *et al.*, 2015). "Continuous simulation" is based on monthly averages of the daily water balance of Equation 5 as used in Figures 6 and 7. The thin dotted lines represent respective ranges that contain 90% of the simulated monthly values.

The analysis of possible future scenarios is crucial for understanding the sensitivity of groundwater recharge formation to climatic changes (Figure 10). In all of the analyzed scenarios, recharge remains limited to the season from October to April. During the opposite recharge-free period, evapotranspiration continues due to the available soil moisture with a minimum of 50 mm in September. Across all scenarios, the variations in both *ET* and *h* remained relatively unaffected throughout the year, averaging 2 mm/day and 150 mm.

In contrast, the recharge rates vary significantly for individual months as well as in terms of the annual average with respect to the base case of 322 mm/day. This lower base case recharge compared to Figure 9 (352 mm/day) is due to the fact that rainfall time series here are randomly generated based on the statistics of Figure 4 for a direct comparison to the change scenarios, while the actual observed time series are used in Figure 9. For scenarios 1 and 2, which imply a 10% reduction in average precipitation, recharge is reduced most significantly to 248 and 222 mm/year, respectively, i.e., by up to over 30% with respect to the base case. In contrast, scenarios 3 and 4 with internally different rainfall statistics but otherwise constant average precipitation, present a slight increase in recharge to 339 and 353 mm/year, respectively, i.e., by up to almost 10% compared to the base case.

Overall, this indicates that due to the large soil water storage capacity in the study region, groundwater recharge is much more sensitive to changes in the precipitation regime than evapotranspiration and soil water content. As a consequence, this implies that impacts on groundwater availability (saturated water table elevation) may be expected to be more severe than on land surface vegetation.

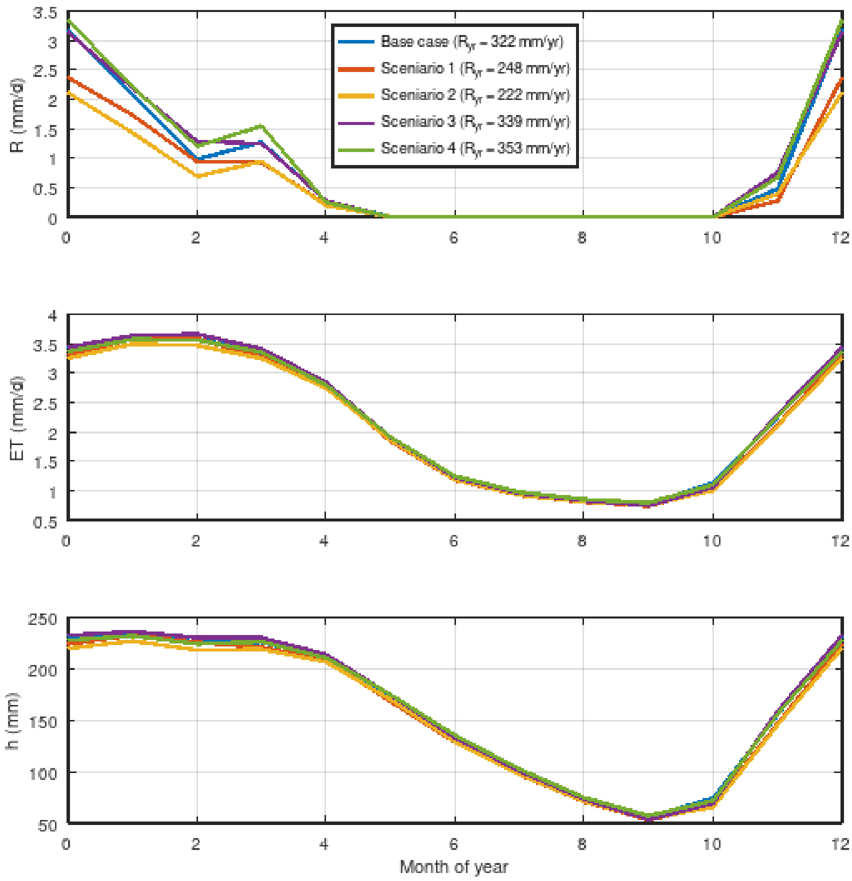

Figure 10. Simulation results for future scenarios. The base case corresponds to Figure 4, while scenario 1 applies a 10% reduction in α, scenario 2 a 10% reduction in λ, scenario 3 a 10% reduction in α with 10% increase in λ, and scenario 4 a 10% increase in α with 10% reduction in λ, all with respect to the base case.

The same approach used to create Figures 4-10 for Gatos station is also applied for the remaining hydrometeorological stations at Arrojado, Arrojolândia, Correntina, and Fazenda Planalto. Based on the strong homogeneity of the soil, climate and native vegetation in the region as well as a lack of more detailed information, we maintain the same critical soil water storage capacity of h_{cr} = 250 mm and the time series of *PET* (Figure 4) for all stations. The corresponding results are available as figures in the online Supplemental Material illustrating that in general, the monthly statistics of *P* as well as the estimated seasonal variabilities in *R*, *ET* and *h* follow a highly uniform pattern across all five stations and methods applied. In particular, recharge remains completely absent everywhere from May to October. This similarity persists for the future scenarios analyzed and is further corroborated by Figure 5 showing that Equation 11 with A = 20 is a reasonable approximation for estimating recharge as a proportion of precipitation in the study area, when soil water carry-over (i.e., seasonality) is neglected.

A spatial trend in the annual mean precipitation is observed, with increasing volumes from east to west, following the altitudinal gradient. This variation is related to the statistical parameters α and λ, for which monthly maps are presented in the Supplementary Material. Average rainfall intensity α shows lower values in the central and eastern regions throughout the year, with highest values concentrated in the west. Daily rainfall probability λ, in turn, displays a seasonal pattern: from February to June, the highest values occur in the western portion, while this pattern reverses in July and August with a relative increase of λ in the central and eastern regions. The averages of observed precipitation and estimated recharge in mm/year for all stations are 1064 and 352 at Gatos, 927 and 257 at Correntina, 990 and 286 at Arrojado, 1081 and 364 at Arrojolândia, and 1258 and 440 at Fazenda Planalto, with interpolated maps presented in Figure 11.

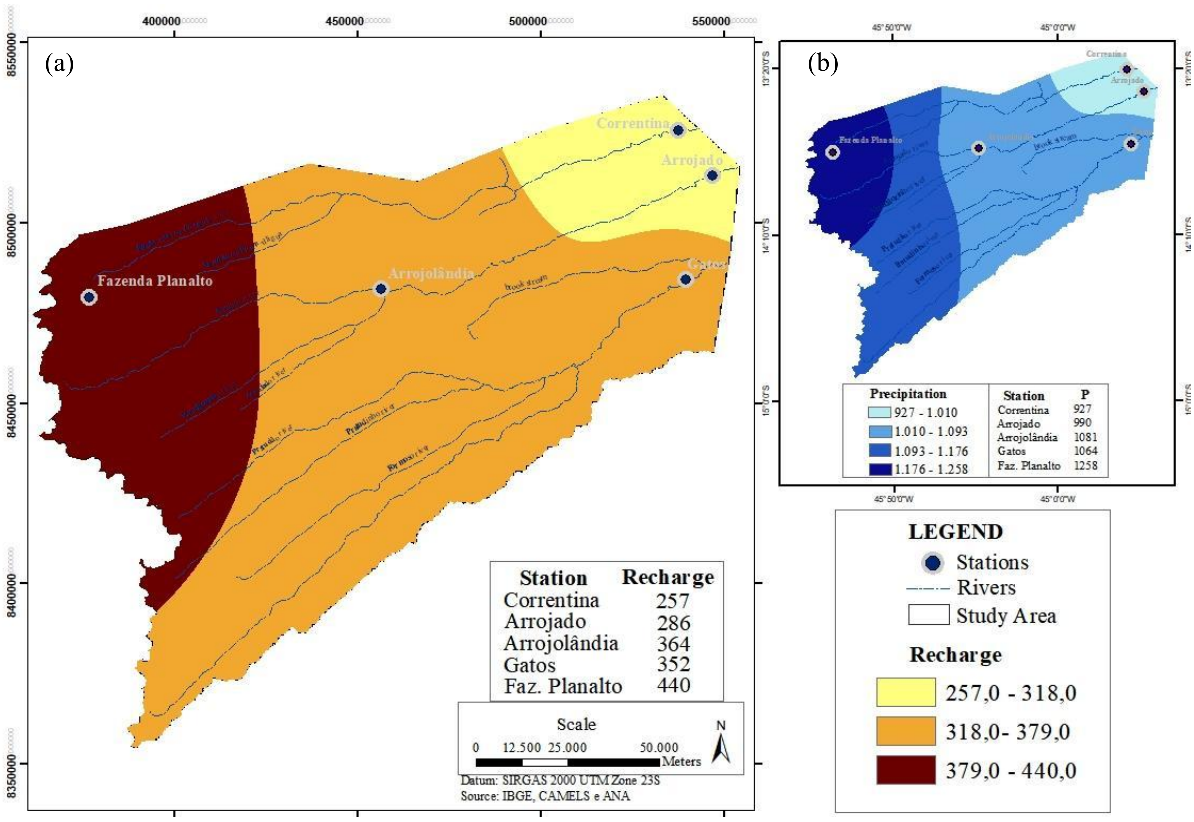

Figure 11. Maps of average (a) simulated average recharge *R* and (b) observed precipitation *P*, both in mm/year. Spatial interpolation between stations by inverse distance weighting (IDW).

4. DISCUSSION

At Gatos and Arrojolândia, recharge amounts to approximately 33% of precipitation. In contrast, Arrojado and Correntina show slightly lower proportions around 28%, while Fazenda Planalto has a slightly higher relative recharge rate of nearly 35% of precipitation. These percentages are somewhat higher than 17% adopted by Oliveira *et al.* (2019) and also than the values obtained at the Gatos station by CPRM *et al.* (2008), which indicated an annual water surplus equivalent to approximately 24% of the mean annual precipitation. However, the absolute recharge value at Correntina compares well to an independent estimate of 230 mm/year for the Corrente River basin (ANA, 2017) and, most importantly, recharge estimates at Gatos, Correntina and Arrojado agree very well with averages of available river discharge data per unit catchment area of 342, 247 and 316 mm/year, respectively (Chagas *et al.*, 2020). Note that while the value for Gatos has already been used in Section 2.5 to partially justify the definition of h_{cr} = 250 mm, the excellent agreement for Correntina and Arrojado is achieved independently, thus providing confidence in the modeling approach adopted.

Across at all stations we also consistently observe (online Supplemental Material) that the simplified emerging threshold-type relationship $R = P - 2$ mm/day (Equation 13) inferred for Gatos from Figure 8 for estimating annual averages of recharge from annual averages of precipitation is generally applicable. Consequently, we identify this relationship as an accurate and practical candidate for estimating annual recharge rates in the study region and discourage the use of percentages, which would still estimate some amount of recharge for $P \leq 2$ mm/day on average over a year.

Related to the specific methods applied in this study, we note that the deterministic soil water balance (Section 2.2) is very easily implemented, but not amenable to making future predictions based on projections of statistical climate parameters (daily input for P and PET are needed). The probabilistic soil water balance (Section 2.3) is convenient for its closed analytical expressions in terms of two dimensionless parameters (aridity index and relative soil water capacity) allowing for a straight-forward graphical representation and sensitivity analysis (Figure 5). However, under conditions of seasonal climatic variability with significant soil water carry-over, as in the present case, it requires a numerical component (Equation 12), which eradicates these advantages. The Monte Carlo approach (Sections 2.4) is basically a numerical extension of the deterministic soil water balance model to include different probabilistic aspects. It is computationally more demanding and requires a random rainfall generator function, but still conceptually simple and flexible, while also providing the option of generating uncertainty bounds about expected predictions.

Where as this methodological assessment is general, it is important to note that the estimated recharge rates and the derived annual relationship ($P = R$ - 2) of this study are limited to the Corrente River basin under natural conditions of vegetation and precipitation. Future work is recommended based on the Monte Carlo method to include the remaining portions of the Urucuia aquifer, as well as explicit consideration of agricultural areas (altered vegetation and rooting depth) with possible irrigation (altered precipitation regime). This could potentially include parametric uncertainty in *hcr*, for example, and in the irrigation regime.

5. CONCLUSIONS

The statistical analysis of long-term precipitation data from five stations in the Corrente River basin of the UAS reveals that the known pronounced seasonality in rainfall is due to synchronous seasonality in both daily precipitation probability and mean intensity. Groundwater recharge as deep percolation from the soil zone is closely linked to this climatic seasonality, being higher during the rainy season and practically null during dry periods, demonstrating a strong correlation with soil water availability. The estimated average recharge rates for different hydrometeorological stations range between 257 mm/year and 440 mm/year, which is consistent with previous estimates for the region and observed long-term average river discharges per unit catchment area. The spatial mapping highlights the western headwater region around Fazenda Planalto station as the area with the highest precipitation and recharge rates, making it a strategic zone for the Urucuia Aquifer's water supply.

The estimated average recharge rates represent approximately 28% to 35% of the average precipitation at each station. However, detailed soil water balance simulations also reveal that annual (from July to June) actual evapotranspiration remains highly steady near 2 mm/day. This suggests the simple relationship $R = P - 2$ (in mm/day with $R \geq 0$; Equation 13) as a practical way to estimate annual recharge directly and accurately from annual precipitation, implying that a quantification by percentage of annual precipitation is inappropriate and not recommended. Similarly, we observe that considering individual months of a year in isolation leads to erroneous results for soil water content, evapotranspiration and recharge, meaning that the pronounced seasonality and soil water carry-over on a seasonal scale cannot be neglected in the Urucuia region.

The stochastic simulation of future scenarios suggests that a decrease in average precipitation due to a decrease in rainfall frequency or intensity leads to an over-proportional decrease in recharge. This strong sensitivity is contrasted by a relative robustness of soil water content and evapotranspiration, which may be attributed to the large rooting depth and associated soil water storage capacity. In overarching terms, this indicates that possibly reduced precipitation rates, as projected for the region, will more significantly impact the deep saturated groundwater resources rather than the soil zone and vegetation.

In summary, this study provides essential methods and information for planning and managing water resources, which are fundamental for the sustainable development of the region. With the growing pressure from irrigated agriculture and the impacts of climate change, it is crucial to adopt conservation strategies, promoting sustainable water use and minimizing the environmental effects of agricultural expansion. Further research and the implementation of public policies are essential to ensure a sustainable future of the Urucuia Aquifer System. Related to the present work in particular, we recommend future investigations focusing on extensions to the remaining portions of the Urucuia region, including agricultural areas with and without irrigation, different rooting depth (crop types) and / or potential evapotranspiration regimes.

6. DATA AVAILABILITY STATEMENT

Data availability not informed.

7. ACKNOWLEDGEMENTS

E.C. Oliveira Souza thanks the Brazilian Federal Agency for Support and Evaluation of Graduate Education (CAPES) for financial support through scholarship no. 88887.659696/2021-00. L.R. Bastos Leal and H. Klammler thank the Brazilian National Council for Scientific and Technological Development (CNPq) for the support provided through grants no. 312977/2021-2 and no. 311333/2021-4, respectively.

8. REFERENCES

ADHIKARI, R. K.; YILMAZ, A. G.; MAINALI, B.; DYSON, P.; IMTEAZ, M. A. Methods of Groundwater Recharge Estimation under Climate Change: A Review. **Sustainability**, v. 14, n. 23, p. 15619, 2022. https://doi.org/10.3390/su142315619

ANA (Brasil). **Sistema Nacional de Informações sobre Recursos Hídricos**. Brasília, 2024. Available: http://www.snirh.gov.br/hidroweb/publico/medicoes_historicas_abas.jsf

ANA (Brasil). **Estudos hidrogeológicos e de vulnerabilidade do Sistema Aquífero Urucuia e proposição de modelo de gestão integrada e compartilhada**: Volume 2 – Hidrogeologia dos sistemas aquíferos Urucuia e Areado. Brasília, 2017. 41-53p. Available: https://metadados.snirh.gov.br/geonetwork/srv/api/records/b26a6c8e-affa-4766-8cb7-ccdaaadb3453/attachments/Volume_2.pdf

AL-NAJJAR, H.; CERIBASI, G.; CEYHUNLU, A. I. Effect of unconventional water resources interventions on the management of Gaza coastal aquifer in Palestine. **Water Supply**, v. 21, n. 8, p. 4205–4220, 2021. https://doi.org/10.2166/ws.2021.170

AL-NAJJAR, H.; CERIBASI, G.; DOGAN, E.; CEYHUNLU, A. I.; ABUALTAYEF, M.; QAHMAN, K. GCMs simulation-based assessment for the response of the Mediterranean Gaza coastal aquifer to climate-induced changes. **Journal of Water and Climate Change**, v. 13, n. 6, p. 2278–2297, 2022. https://doi.org/10.2166/wcc.2022.339

BARBOSA, N. S.; LEAL, L. R. B.; MELLO, J. C.; PEIXINHO, M. A. L.; SANTOS, C. B.; SANTOS, R. L. S. *et al.* Modelo hidrogeológico conceitual do Sistema Aquífero Urucuia Centro-Ocidental, Brasil. **Águas Subterrâneas**, v. 31, n. 1, p. 1-19, 2017. https://doi.org/10.14295/ras.v31i1.28524

BECKE, A. L.; SOLÓRZANO-RIVAS, S. C.; WERNER, A. D. The water table fluctuation method of recharge estimation: A review. **Advances in Water Resources**, v. 189, p. 104635, 2024. https://doi.org/10.1016/j.advwatres.

BOTTER, G.; PORPORATO, A.; RODRIGUEZ-ITURBE, I.; RINALDO, A. Basin-scale soil moisture dynamics and the probabilistic characterization of carrier hydrologic flows: Slow, leaching-prone components of the hydrologic response. **Water Resources Research**, v. 43, n. 2, 2007. https://doi.org/10.1029/2006WR005043 .

BRASIL. Ministério da Agricultura, Pecuária e Abastecimento. **Projeções do Agronegócio**: Brasil 2017/18 a 2027/28 projeções de longo prazo. Brasília, 2018. 112 p.

CAMPOS, J. E. G.; DARDENNE, M. A. Estratigrafia e sedimentação da Bacia Sanfranciscana: uma revisão. **Revista Brasileira de Geociências**, v. 27, n. 3, p. 269-282, set. 1997. https://doi.org/10.25249/0375-7536.1997269282

CANADELL, J.; JACKSON, R. B.; EHLERINGER, J. R.; MOONEY, H. A.; SALA, O. E.; SCHULZE, E.-D. Maximum rooting depth of vegetation types at the global scale. **Oecologia,** v. 108, p. 583–595, 1996. https://doi.org/10.1007/BF00329030

CHAGAS, V. B. P. *et al.* CAMELS-BR: hydrometeorological time series and landscape attributes for 897 catchments in Brazil. **Earth System Science Data**, v. 12, p. 2075–2096, 2020. https://doi.org/10.5194/essd-12-2075-2020

COELHO, L. Ninguém vai morrer de sede nas margens do rio. **Prato Cheio**, São Paulo: O Joio e O Trigo, temp. 7, ep. 6, 2024. Podcast. Available: https://ojoioeotrigo.com.br/podcast/prato-cheio

CPRM; SERVIÇO GEOLÓGICO DO BRASIL; UFBA. **Caracterização hidroquímica e de vulnerabilidade**: Meta D – Hidrogeologia da Bacia Sedimentar do Urucuia: Bacias Hidrográficas dos Rios Arrojado e Formoso. Salvador: Rede Cooperativa de Pesquisa – Comportamento das Bacias Sedimentares da Região Semi-Árida do Nordeste Brasileiro, out. 2007.

EILERS, V. H. M. Estimativa de recarga de águas subterrâneas utilizando o método do balanço hídrico. In: CONGRESSO BRASILEIRO DE ÁGUAS SUBTERRÂNEAS, 13., 2004, Belo Horizonte. **Anais[...]** São Paulo: ABAS, 2004. p. 1-19.

FENG, X.; PORPORATO, A.; RODRIGUEZ-ITURBE, I. Stochastic soil water balance under seasonal climates. **Proceedings A**, v. 471, p. 20140623, 2015. https://doi.org/10.1098/rspa.2014.0623

GASPAR, M. T. P. **Sistema Aquífero Urucuia: Caracterização regional e propostas de gestão.** 2006. 156f. Tese (Doutorado em Geologia) – Universidade de Brasília, Brasília, 2006.

GASPAR, M. T. P.; CAMPOS, J. E. G. O Sistema Aquífero Urucuia. **Revista Brasileira de Geociências**, v. 37, n. 4, suplemento, p. 1068-1078, dez. 2007.

GASPAR, M. T. P.; CAMPOS, J. E. G.; CADAMURO, A. L. M. Condições de infiltração em solos na região de recarga do sistema aquífero Urucuia no oeste da Bahia sob diferentes condições de uso. **Revista Brasileira de Geociências**, v. 37, n. 3, p. 542-550, 2007.

GEBRU, A. B.; GEBREYOHANNE, T.; KAHSAY, G. H.; GRUM, B. The dilemma of choosing appropriate groundwater recharge estimation methods in Ethiopia: A systematic review of the existing methods. **Groundwater for Sustainable Development**, v. 27, p. 101358, 2024. https://doi.org/10.1016/j.gsd.2024.101358

HIRATA, R.; SUHOGUSOFF, A.; SUSKO MARCELLINI, S.; VILLAR, P. C.; MARCELLINI, L. **As águas subterrâneas e sua importância ambiental e socioeconômica para o Brasil.** São Paulo: Universidade de São Paulo/Instituto de Geociências, 2019. 158 p.

IPCC. Climate Change 2022: Impacts, Adaptation and Vulnerability. *In*: PÖRTNER, H.-O. *et al.* (org.). **Contribution of Working Group II to the Sixth Assessment Report of the Intergovernmental Panel on Climate Change**. Chapter 4 – Water. Cambridge: Cambridge University Press, 2022. Available at: https://www.ipcc.ch/report/ar6/wg2/chapter/chapter-4/

KUMAR, P. J. S.; SCHNEIDER, M.; ELANGO, L. The state-of-the-art estimation of groundwater recharge and water balance with a special emphasis on India: A critical review. **Sustainability**, v. 14, n. 1, 340 p, 2022. https://doi.org/10.3390/su14010340

LOBO-FERREIRA, J. P.; LEITÃO, T. E.; OLIVEIRA, M. M. Portugal's river basin management plans: groundwater innovative methodologies, diagnosis, and objectives. **Environmental Earth Sciences**, 2014. https://doi.org/10.1007/s12665-014-3462-8

MANTOVANI, E. C.; SILVA JÚNIOR, A. G. da; COSTA, M. H.; MARQUES, E. A. G.; SILVA JÚNIOR, G. C. da; PRUSKI, F. F. **Estudo do potencial hídrico da Região Oeste da Bahia: quantificação e monitoramento da disponibilidade dos recursos do Aquífero Urucuia e superficiais nas bacias dos rios Grande, Corrente e Carinhanha**. Relatório técnico final. Viçosa: Universidade Federal de Viçosa, 2019.

MIRANDA, E. E.; MAGALHÃES, L. A.; CARVALHO, C. A. **Proposta de delimitação territorial do MATOPIBA**. Nota Técnica 1, GITE – Grupo de Inteligência Territorial Estratégia, Campinas, SP: Embrapa, 2014. 18 p. Available at: https://ainfo.cnptia.embrapa.br/digital/bitstream/item/139202/1/NT1-DelimitacaoMatopiba.pdf

OLIVEIRA, R. S.; BEZERRA, L.; DAVIDSON, E. A.; PINTO, F.; KLINK, C. A.; NEPSTAD, D. C. *et al.* Deep root function in soil water dynamics in Cerrado savannas of central Brazil. **Functional Ecology**, v. 19, p. 574-581, 2005. https://doi.org/10.1111/j.1365-2435.2005.01003.x

OLIVEIRA, L. T.; KLAMMLER, H.; LEAL, L. R. B.; GRISSOLIA, E. M. Analysis of the long-term effects of groundwater extraction on the water balance in part of the Urucuia Aquifer System in Bahia – Brazil. **Revista Ambiente & Água**, v. 14, n. 6, e2390, 2019. https://doi.org/10.4136/ambi-agua.2390

OLIVEIRA, L. T.; KLAMMLER, H.; LEAL, L. R. B.; GRISSOLIA, E. M. Balanço hídrico transitório do aquífero Urucuia meridional na Bahia. **Águas Subterrâneas**, v. 34, n. 3, p. 325-339, 2020. https://doi.org/10.14295/ras.v34i3.29915

OLIVEIRA, S. D. M. Conflitos pela água no Oeste da Bahia: por uma abordagem ontológica dos conflitos socioambientais. *In*: CONGRESSO BRASILEIRO DE SOCIOLOGIA, 20., 2021, Belém. **Anais[...]** Belém: Universidade Federal do Pará, 2021. p. 1-23.

OTHMAN, A.; ABDELRADY, A.; MOHAMED, A. Monitoring mass variations in Iraq using time-variable gravity data. **Remote Sensing**, v. 14, n. 14, p. 3346, 2022. https://doi.org/10.3390/rs14143346

PEREIRA, B. H. F. **Projeções de recarga hídrica para o Sistema Aquífero Urucuia (Bahia) no período 2041-2060**. 2021. 88f. Dissertação (Mestrado em Meteorologia) – Universidade Federal do Rio de Janeiro, Rio de Janeiro, 2021.

POLIZEL, S. P. *et al.* Land use changes and compliance with environmental legislation in the MATOPIBA region of Brazil. **Land Use Policy**, v. 111, p. 105713, 2021. https://doi.org/10.1016/j.landusepol.2021.105713

PONTES, L. M.; COELHO, G.; MELLO, C. R.; SILVA, A. M.; OLIVEIRA, G. C.; VIOLA, M. R. Avaliação de modelo de balanço hídrico com base na estimativa da recarga potencial. **Revista Ambiente & Água**, v. 11, n. 4, p. 915–928, 2016. https://doi.org/10.4136/ambi-agua.1856

PORPORATO, A.; DALY, E.; RODRIGUEZ-ITURBE, I. Soil water balance and ecosystem response to climate change. **The American Naturalist**, v. 164, n. 5, p. 625-632, 2004. https://doi.org/10.1086/424970

POUSA, R.; COSTA, M. H.; PIMENTA, F. M.; FONTES, V. C.; BRITO, V. F. A.; CASTRO, M. Climate Change and Intense Irrigation Growth in Western Bahia, Brazil: The Urgent Need for Hydroclimatic Monitoring. **Water,** v. 11, n. 933, p. 1-21, 2019. https://doi.org/10.3390/w11050933

RAWITSCHER, F. K.; FERRI, M. G.; RACHID, M. Profundidade dos solos e vegetação em campos cerrados do Brasil Meridional. **Anais da Academia Brasileira de Ciências**, v. 15, p. 267-294, 1943.

SCANLON, B.; HEALY, R.; COOK, P. Choosing appropriate techniques for quantifying groundwater recharge. **Hydrogeology Journal**, v. 10, n. 1, p. 18-39, 2002. https://doi.org/10.1007/s10040-001-0176-2

THORNTHWAITE, C. W. An approach toward a rational classification of climate. **Geographical Review**, v. 38, n. 1, p. 55–94, 1948. https://doi.org/10.2307/210739

THORNTHWAITE, C. W.; MATHER, J. R. **The water balance**. Centerton: Drexel Institute of Technology, 1955.

TOUHAMI, I.; ANDREU, J. M.; CHIRINO, E.; SÁNCHEZ, J. R.; PULIDO-BOSCH, A.; MARTÍNEZ-SANTOS, P. *et al.* Comparative performance of soil water balance models in computing semi-arid aquifer recharge. **Hydrological Sciences Journal**, v. 59, n. 1, p. 193–203, 2014. https://doi.org/10.1080/02626667.2013.802094

SUPPLEMENTAL MATERIAL

Figures S1-S28: Results of Figures 3, 4, 6, 7, 8, 9 and 10 of the main text for the other stations at Arrojado, Arrojolândia, Correntina and Fazenda Planalto (see Figure 2).

Figures S29-S32: Monthly maps of the study area for precipitation *P*, probability of rainy days *λ*, average rainfall intensity on rainy days *α*, and estimated recharge *R*.

ARROJADO STATION

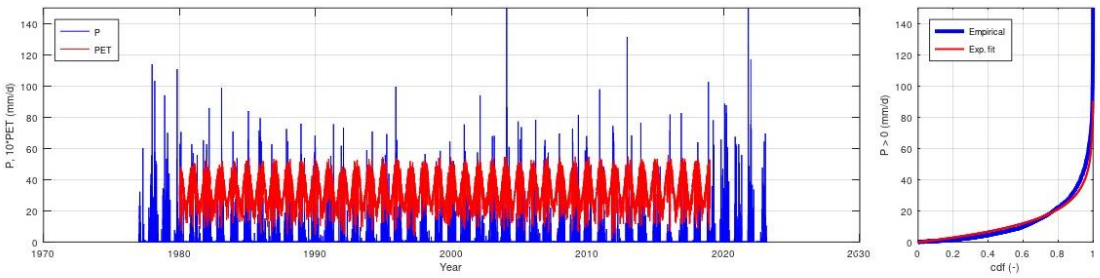

Figure S1. Same as Figure 3, but for Arrojado station.

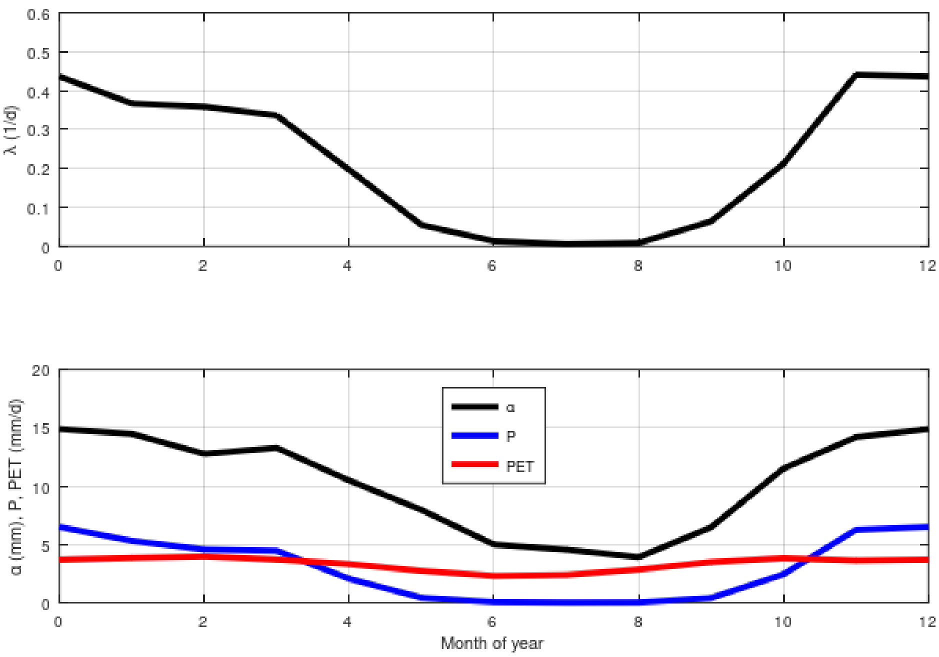

Figure S2. Same as Figure 4, but for Arrojado station.

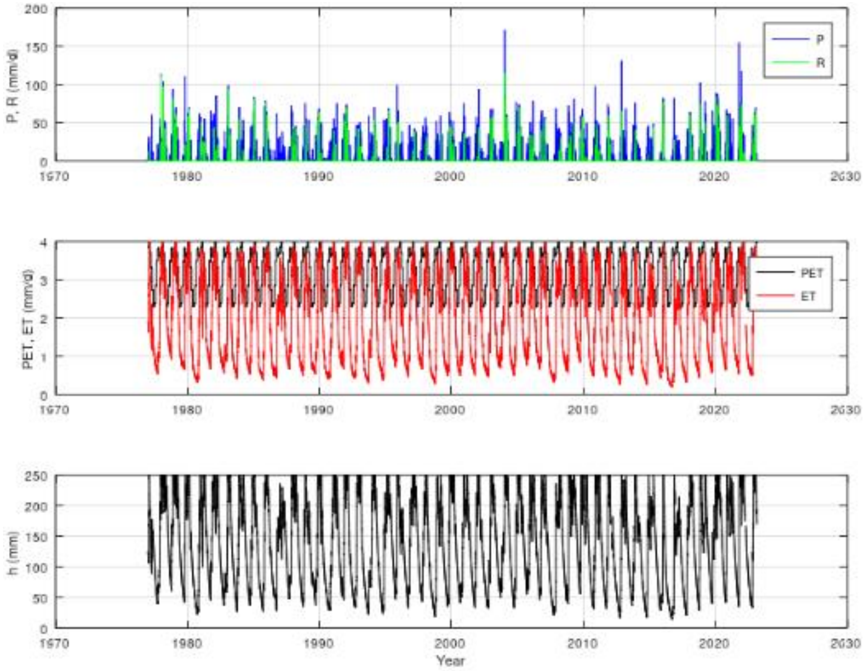

Figure S3. Same as Figure 6, but for Arrojado station.

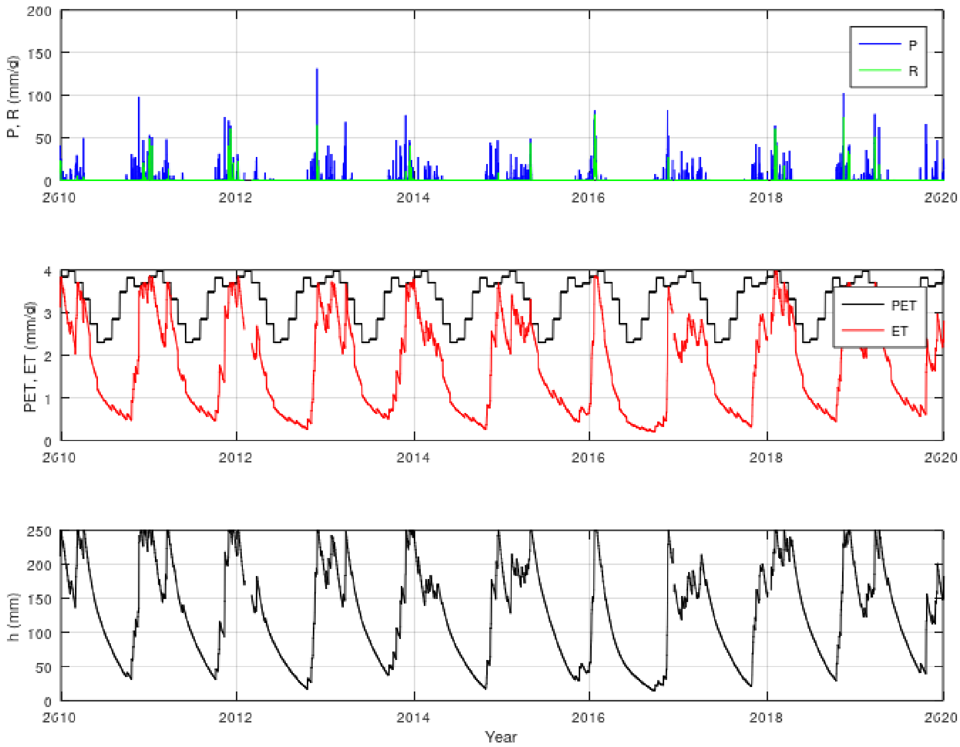

Figure S4. Same as Figure 7, but for Arrojado station.

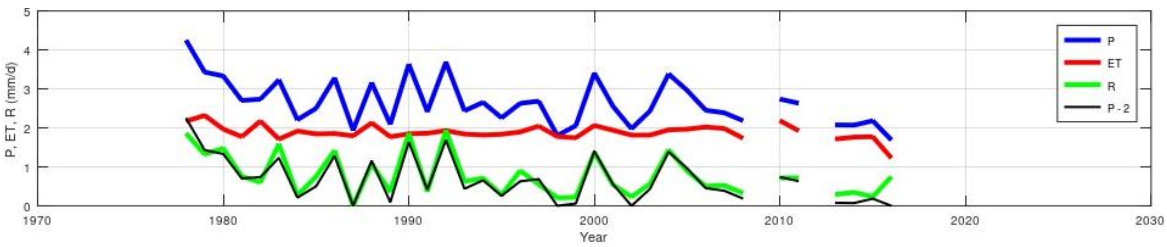

Figure S5. Same as Figure 8, but for Arrojado station.

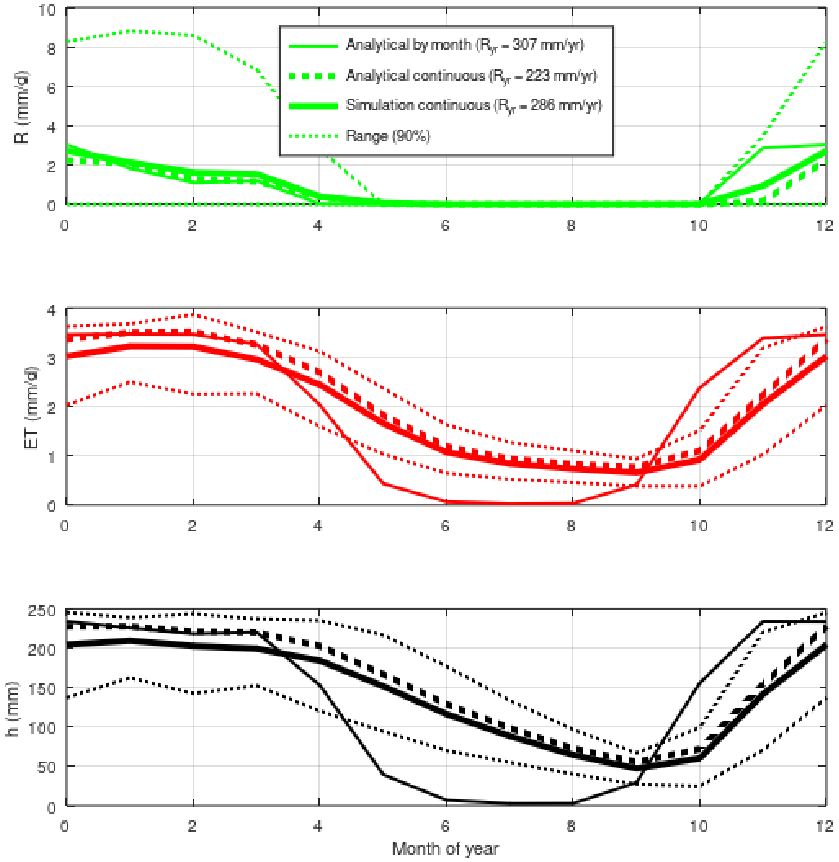

Figure S6. Same as Figure 9, but for Arrojado station.

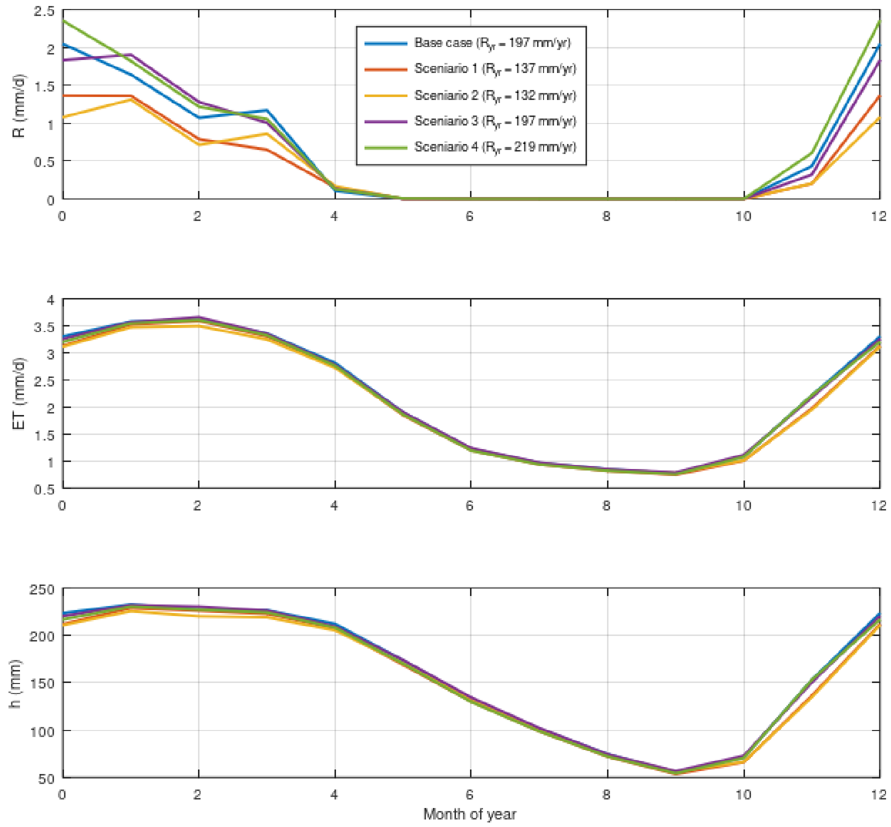

Figure S7. Same as Figure 10, but for Arrojado station.

ARROJOLÂNDIA STATION

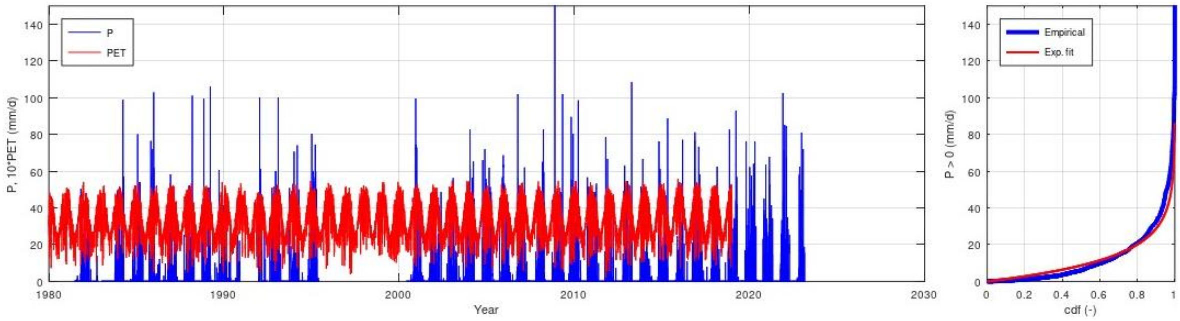

Figure S8. Same as Figure 3, but for Arrojolândia station.

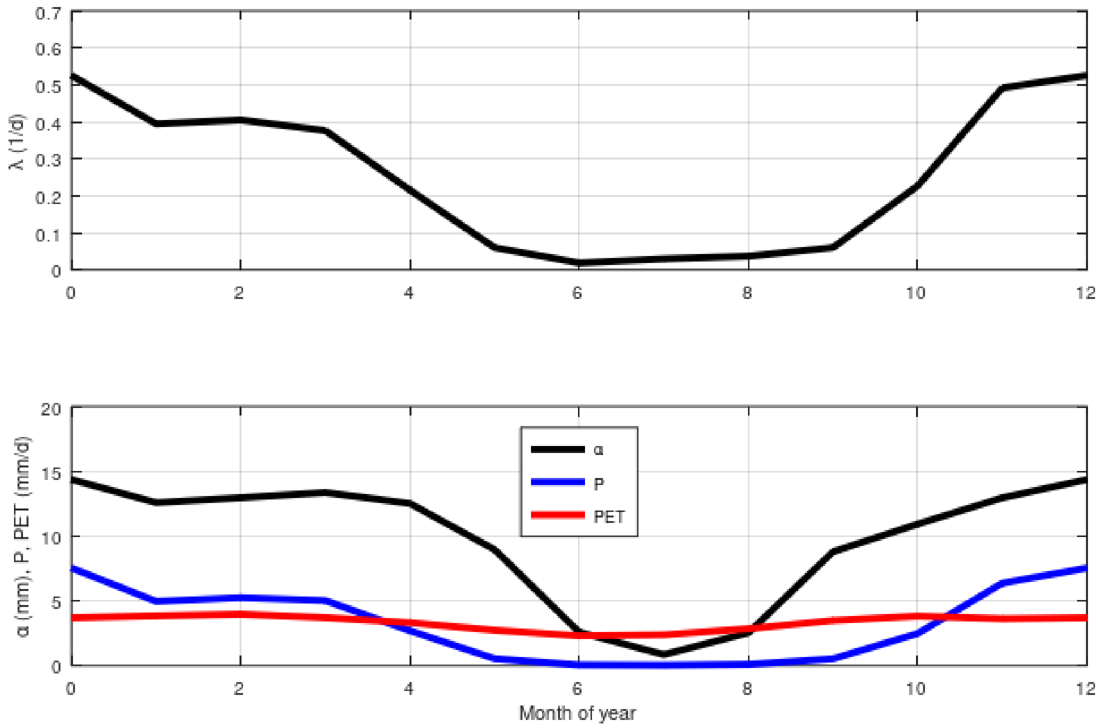

Figure S9. Same as Figure 4, but for Arrojolândia station.

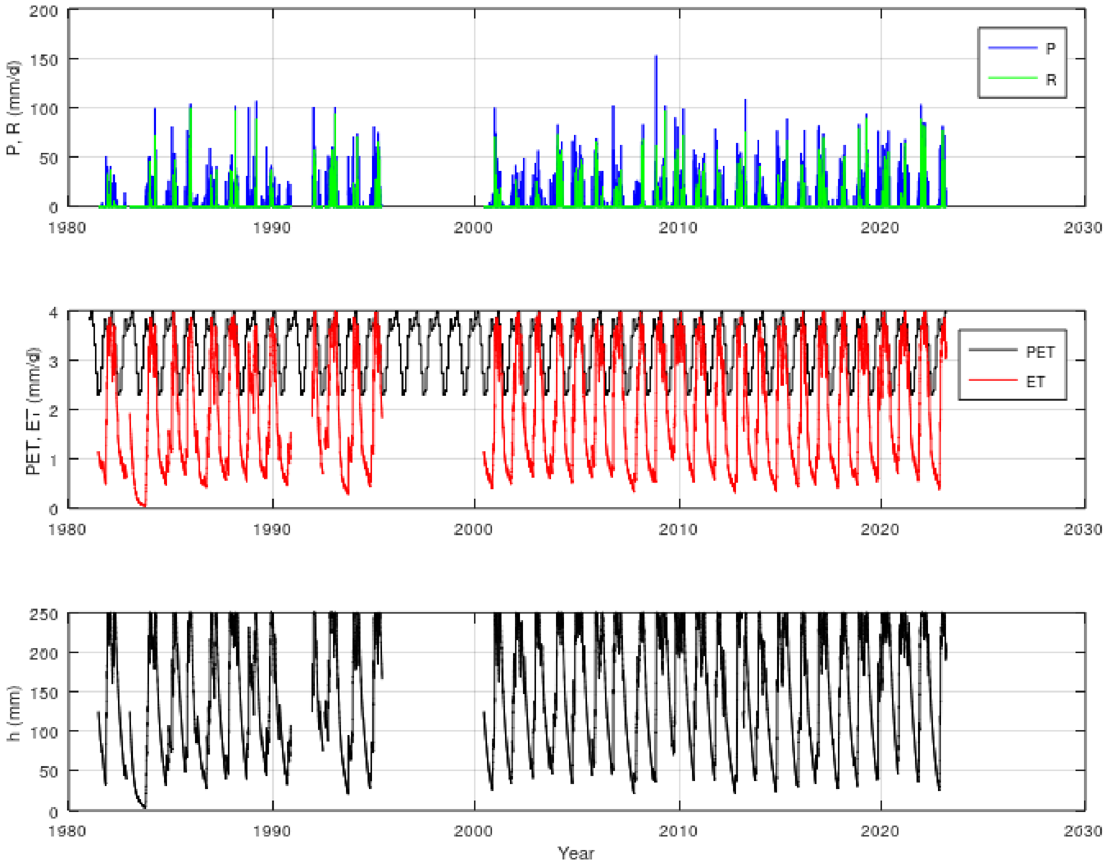

Figure S10. Same as Figure 6, but for Arrojolândia station.

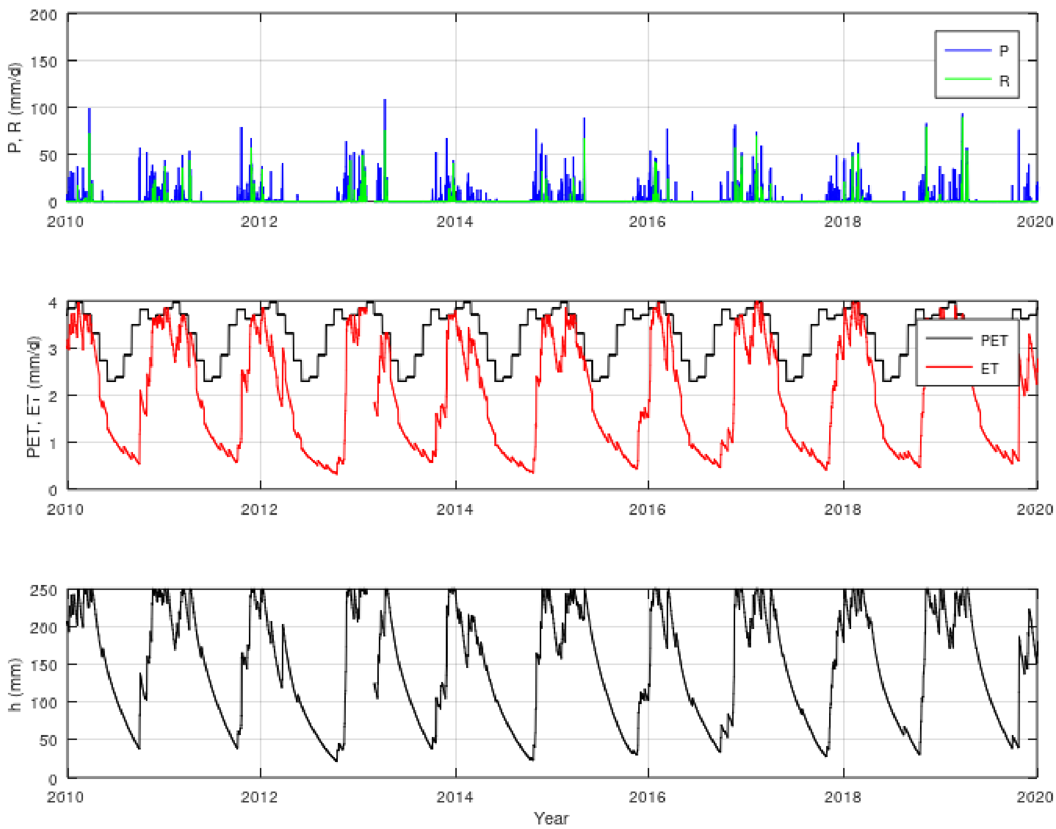

Figure S11. Same as Figure 7, but for Arrojolândia station.

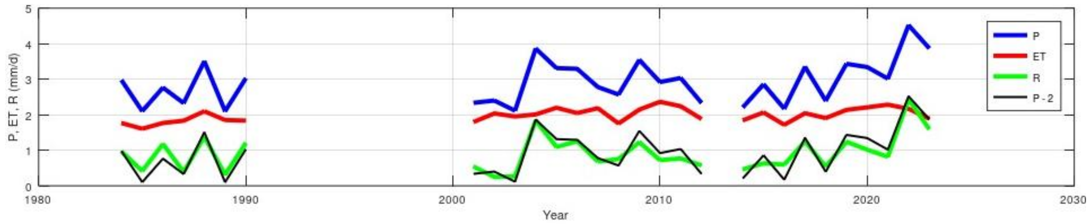

Figure S12. Same as Figure 8, but for Arrojolândia station.

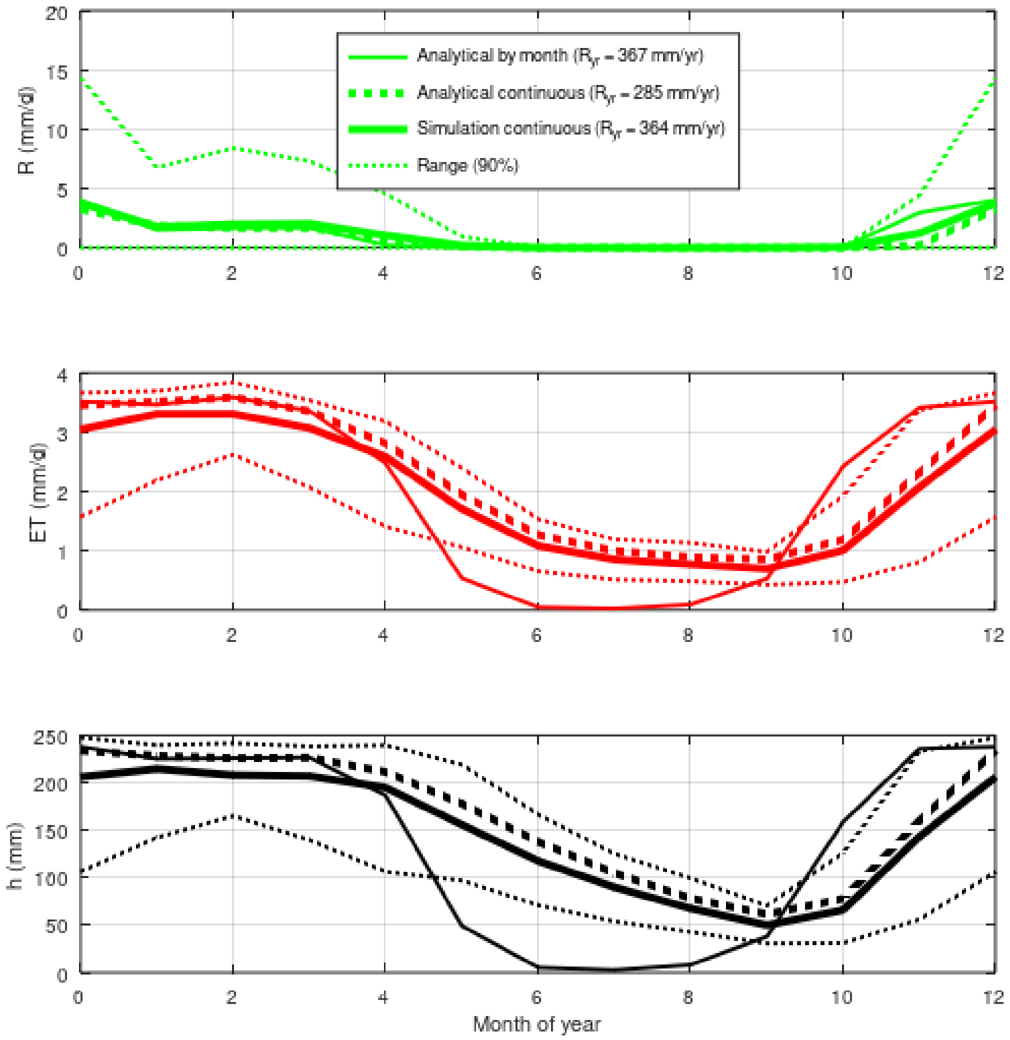

Figure S13. Same as Figure 9, but for Arrojolândia station.

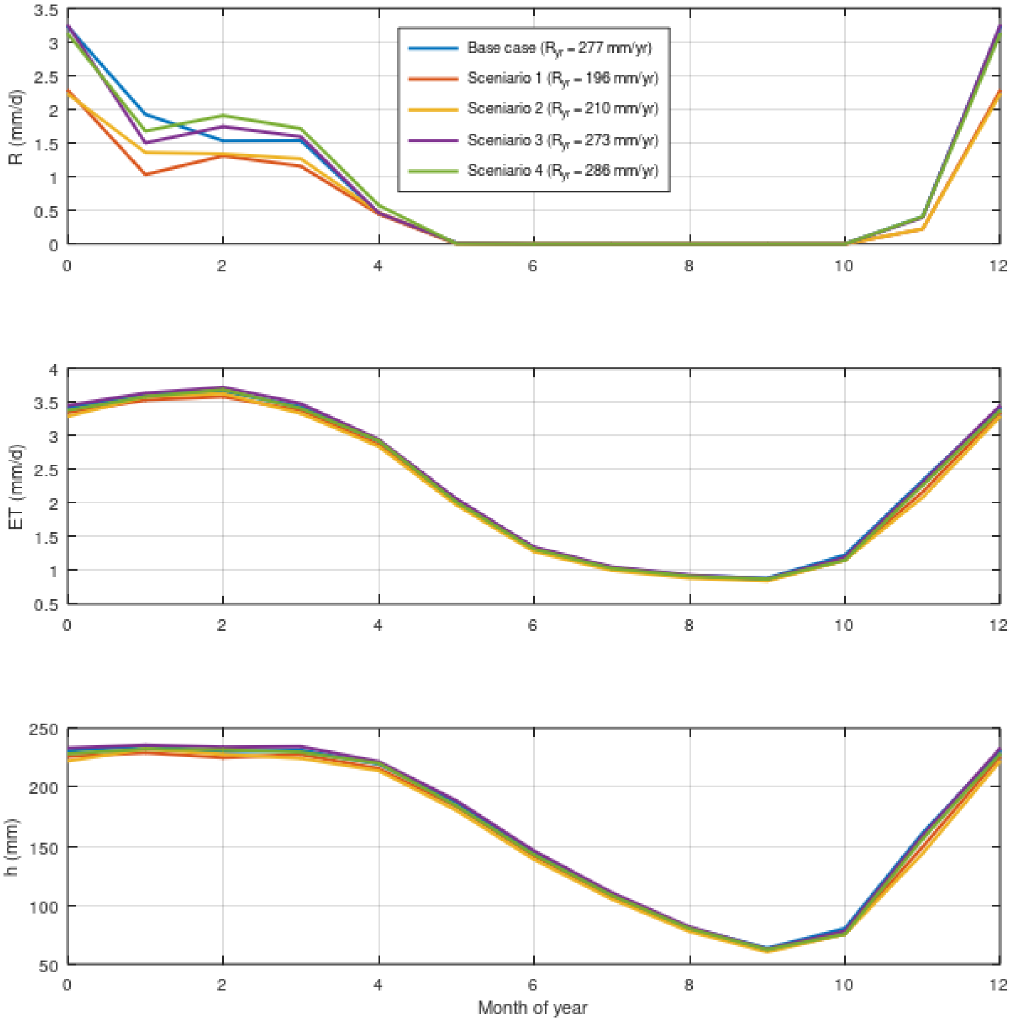

Figure S14. Same as Figure 10, but for Arrojolândia station.

CORRENTINA STATION

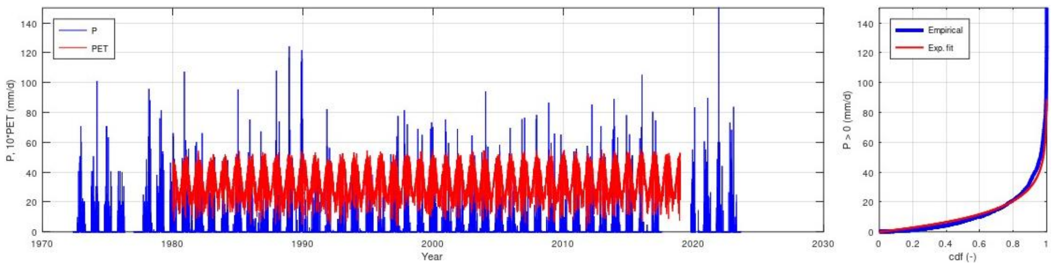

Figure S15. Same as Figure 3, but for Correntina station.

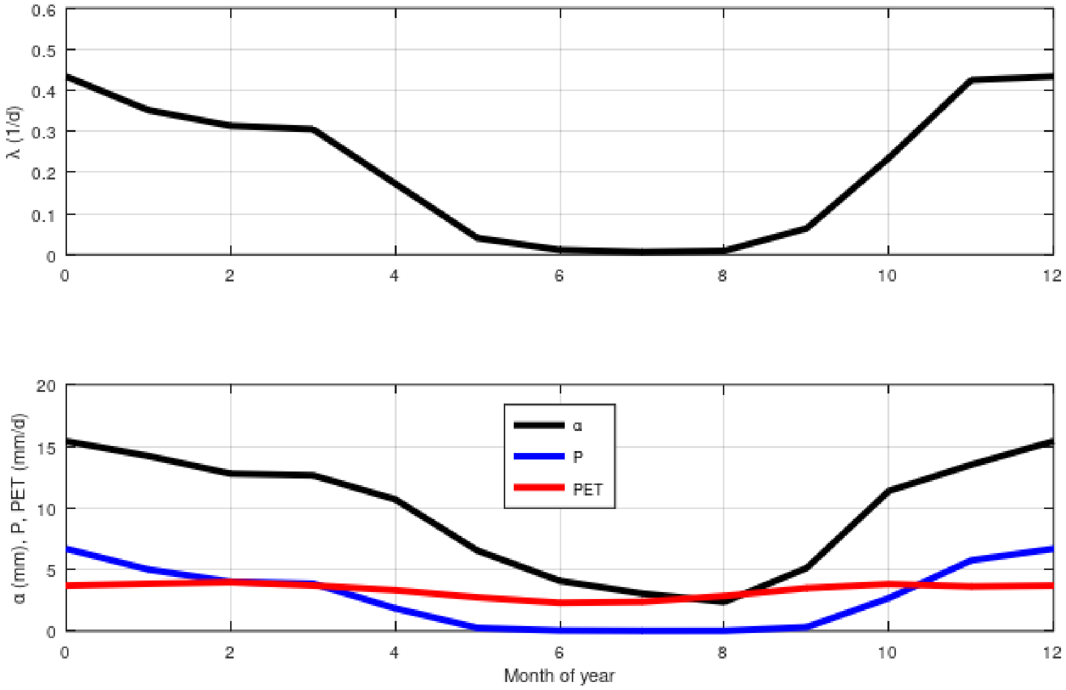

Figure S16. Same as Figure 4, but for Correntina station.

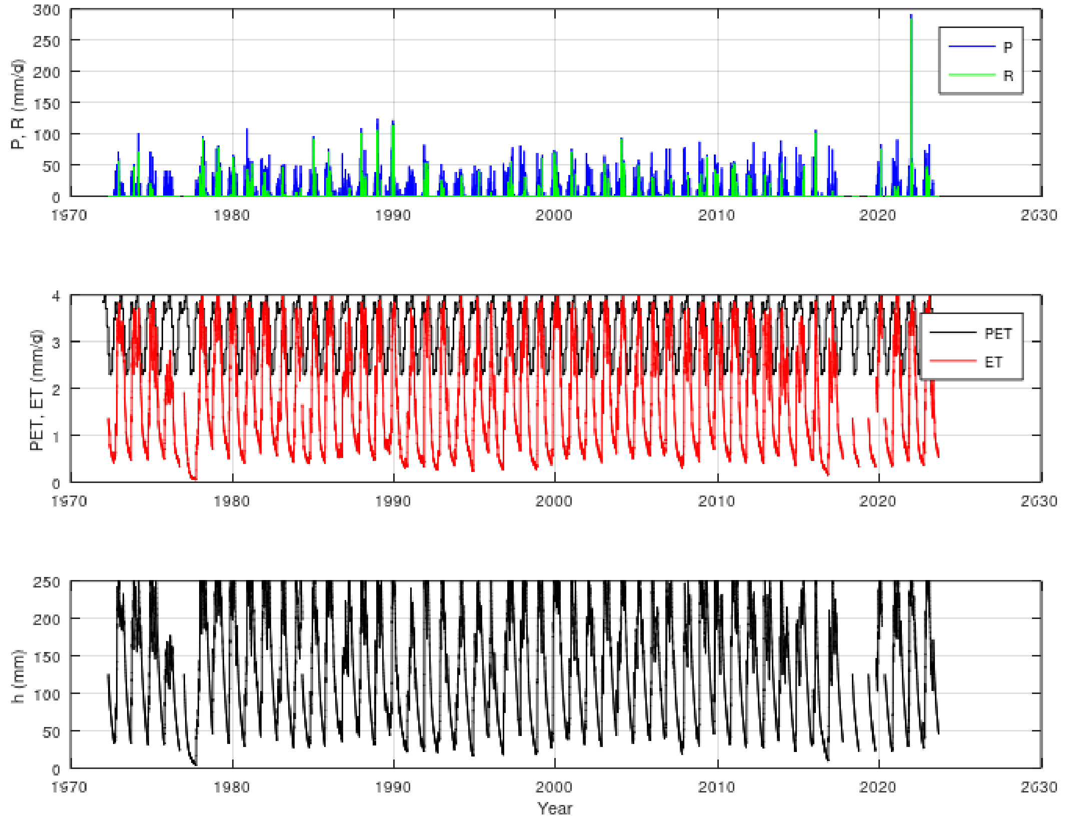

Figure S17. Same as Figure 6, but for Correntina station.

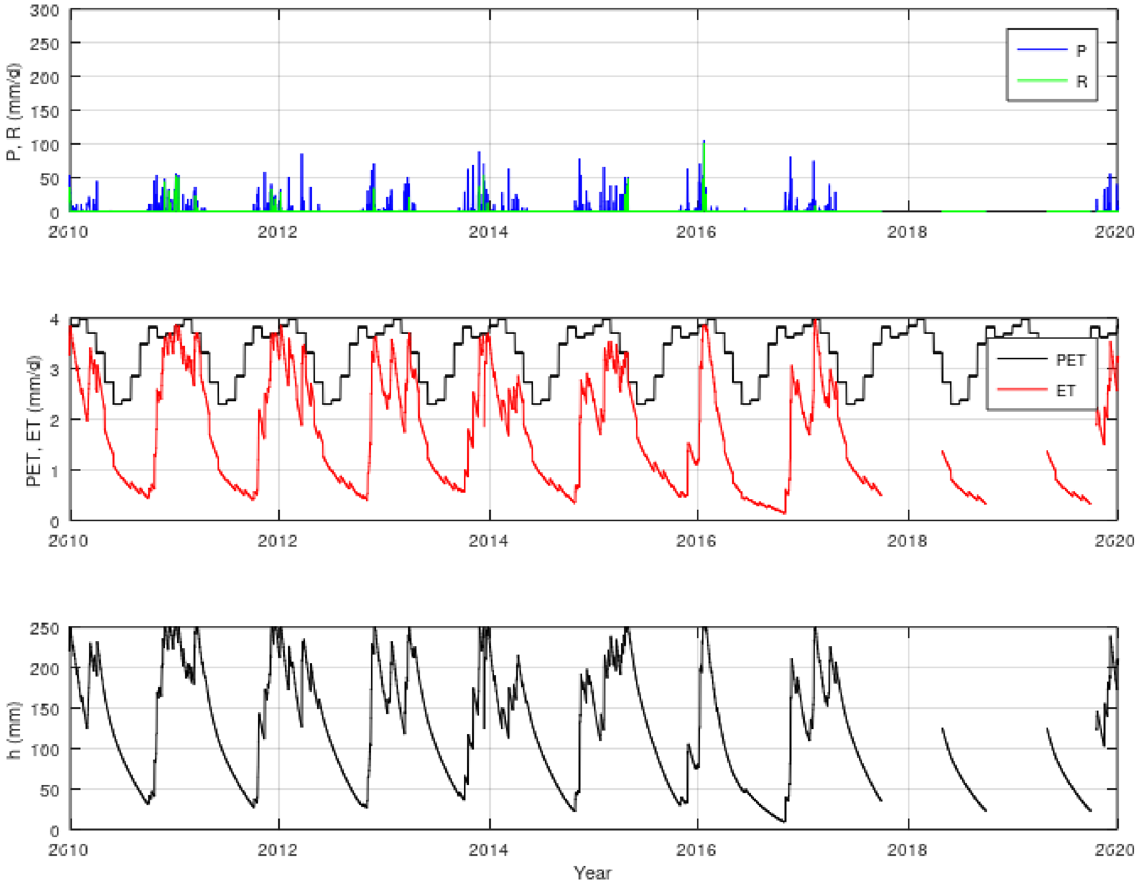

Figure S18. Same as Figure 7, but for Correntina station.

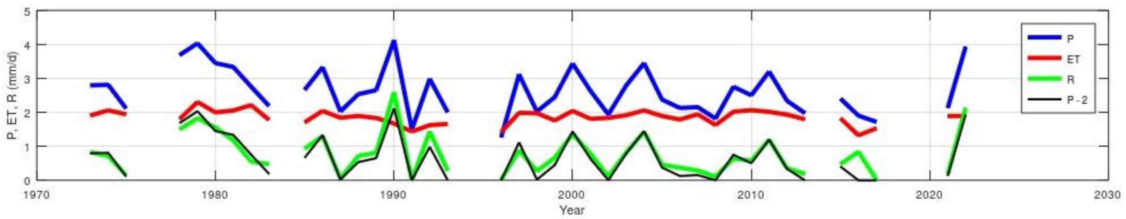

Figure S19. Same as Figure 8, but for Correntina station.

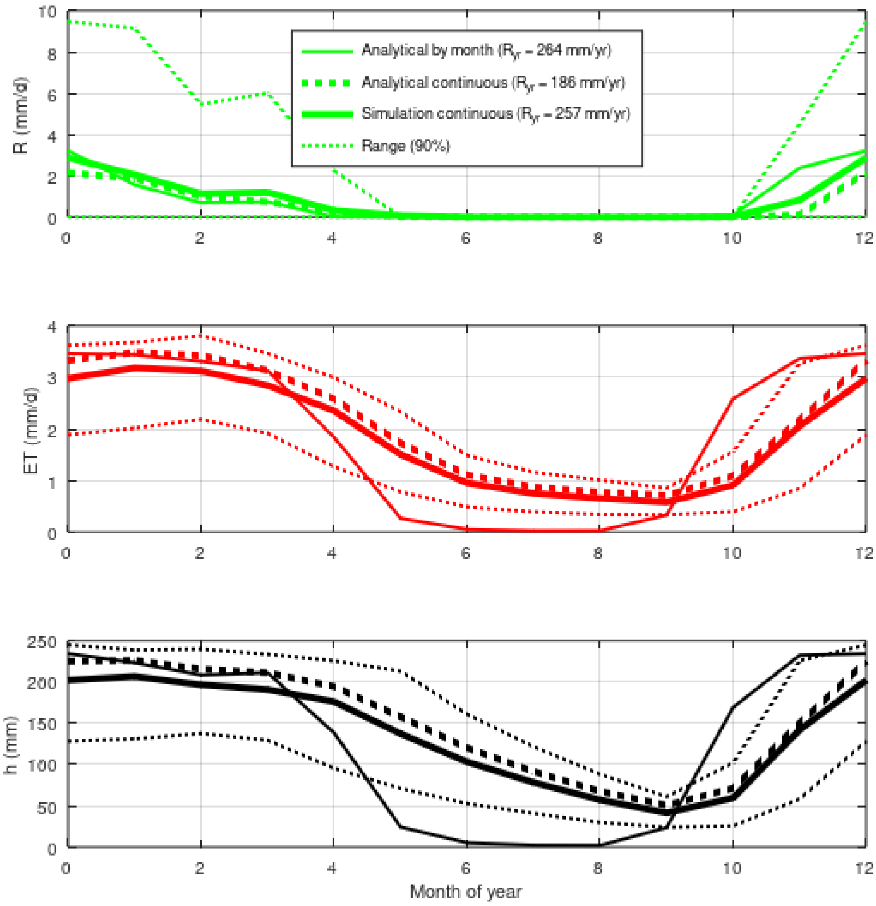

Figure S20. Same as Figure 9, but for Correntina station.

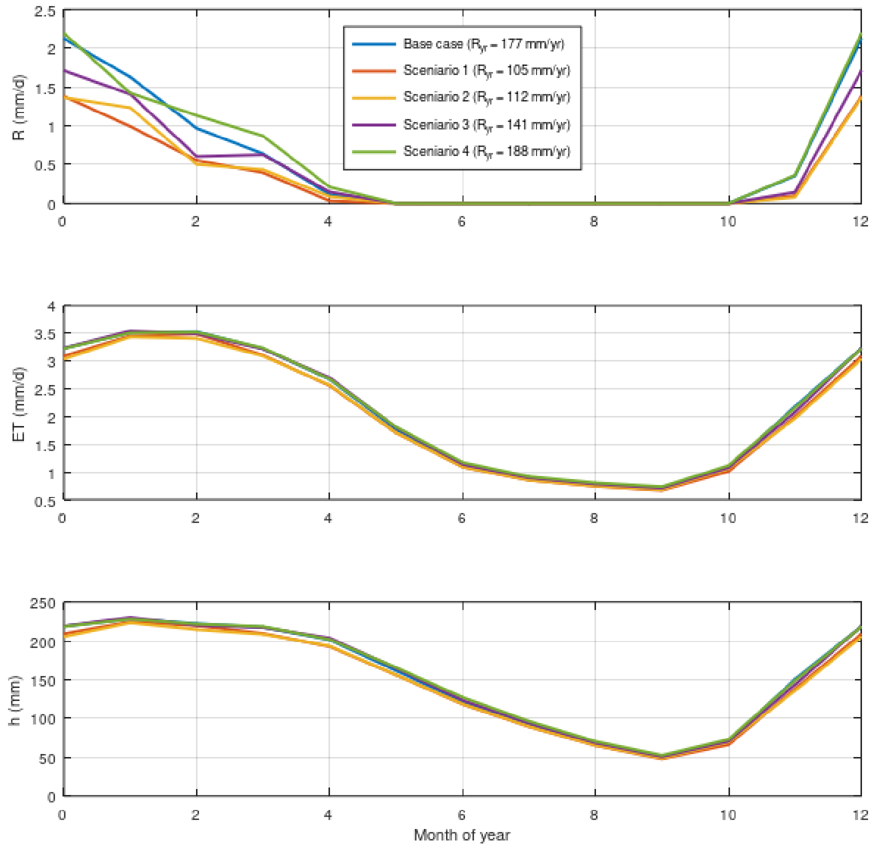

Figure S21. Same as Figure 10, but for Correntina station.

FAZENDA PLANALTO STATION

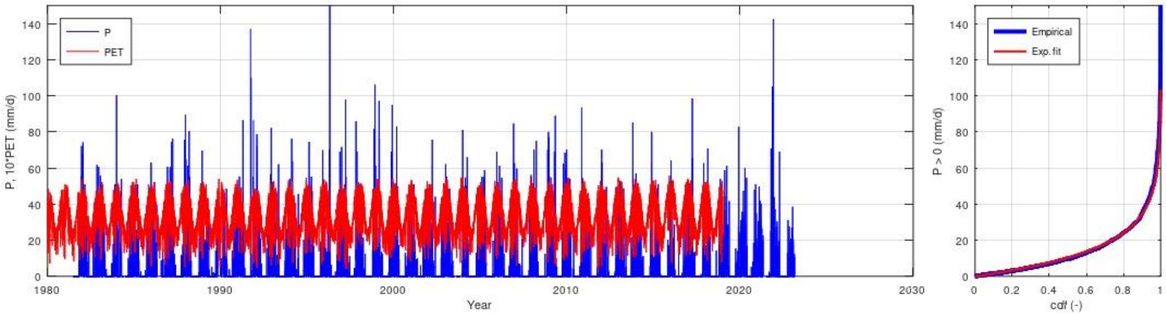

Figure S22. Same as Figure 3, but for Fazenda Planalto station.

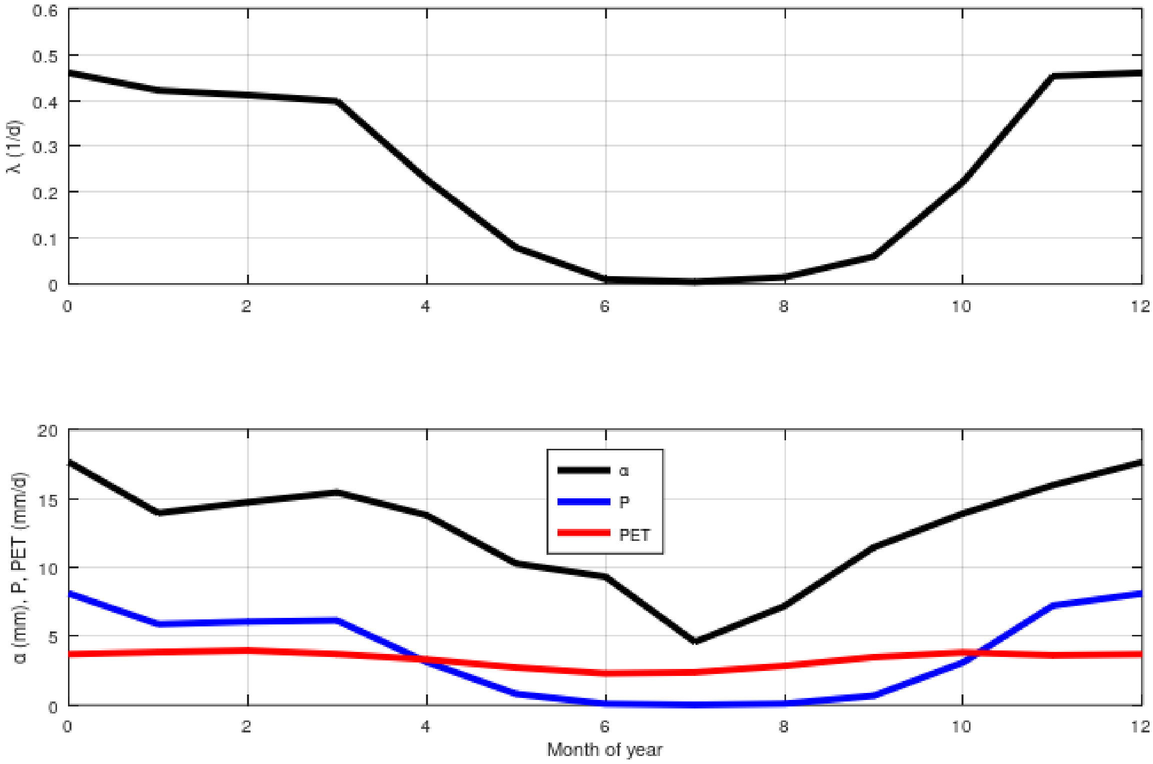

Figure S23. Same as Figure 4, but for Fazenda Planalto station.

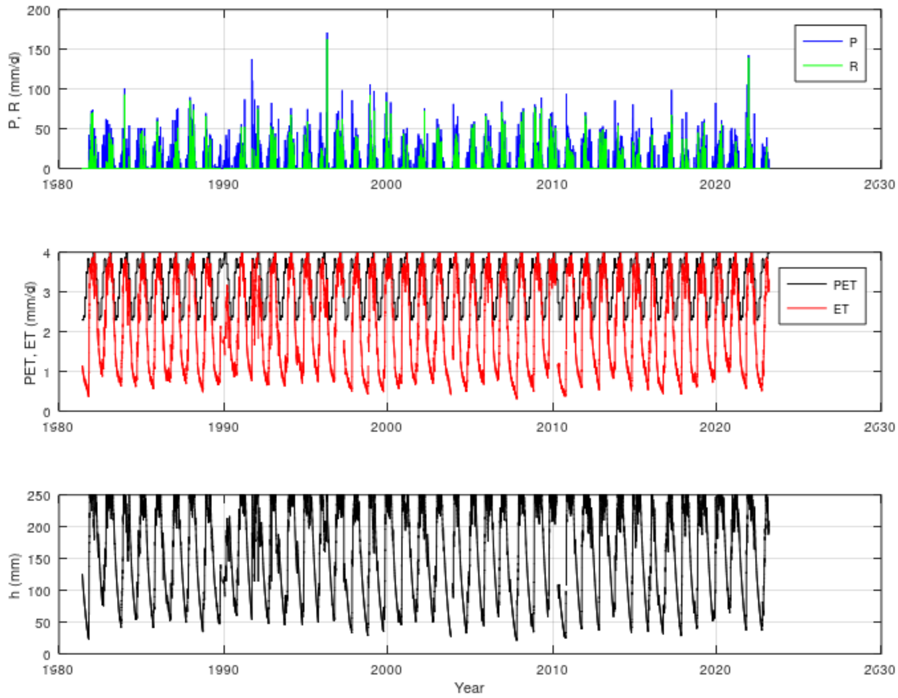

Figure S24. Same as Figure 6, but for Fazenda Planalto station.

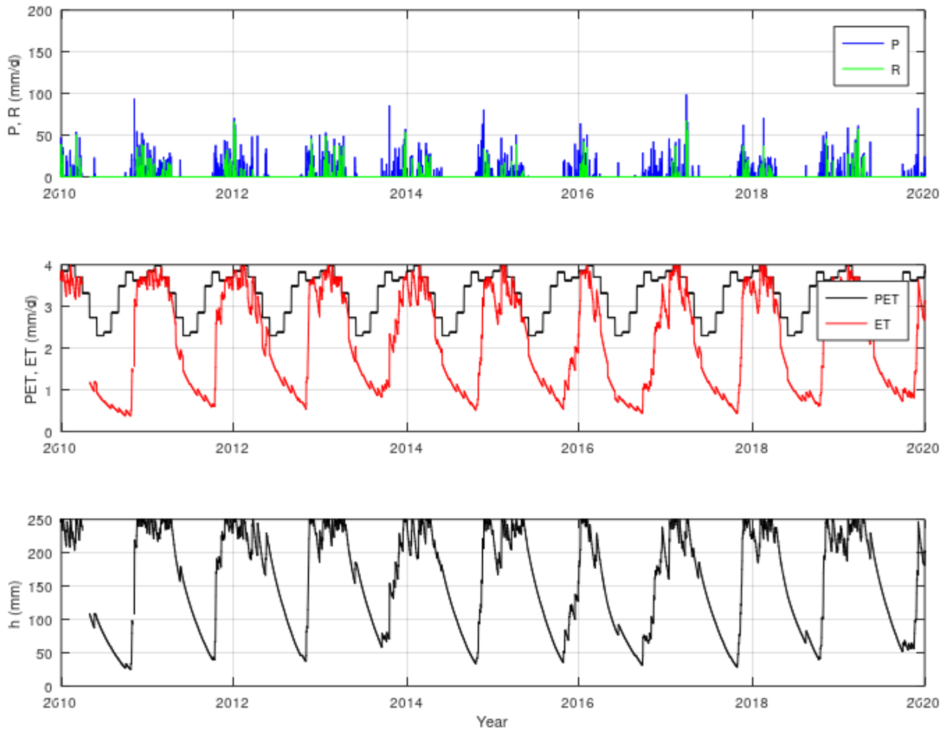

Figure S25. Same as Figure 7, but for Fazenda Planalto station.

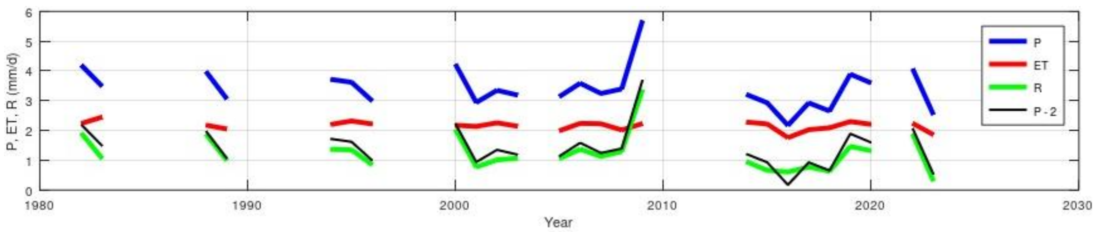

Figure S26. Same as Figure 8, but for Fazenda Planalto station.

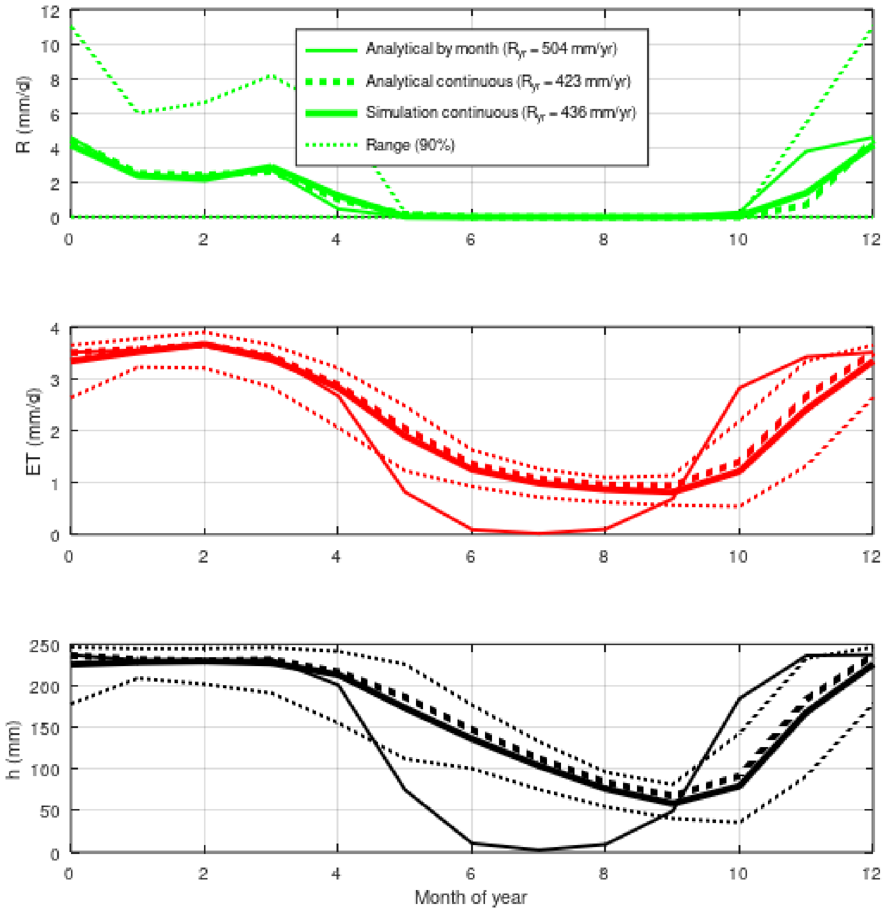

Figure S27. Same as Figure 9, but for Fazenda Planalto station.

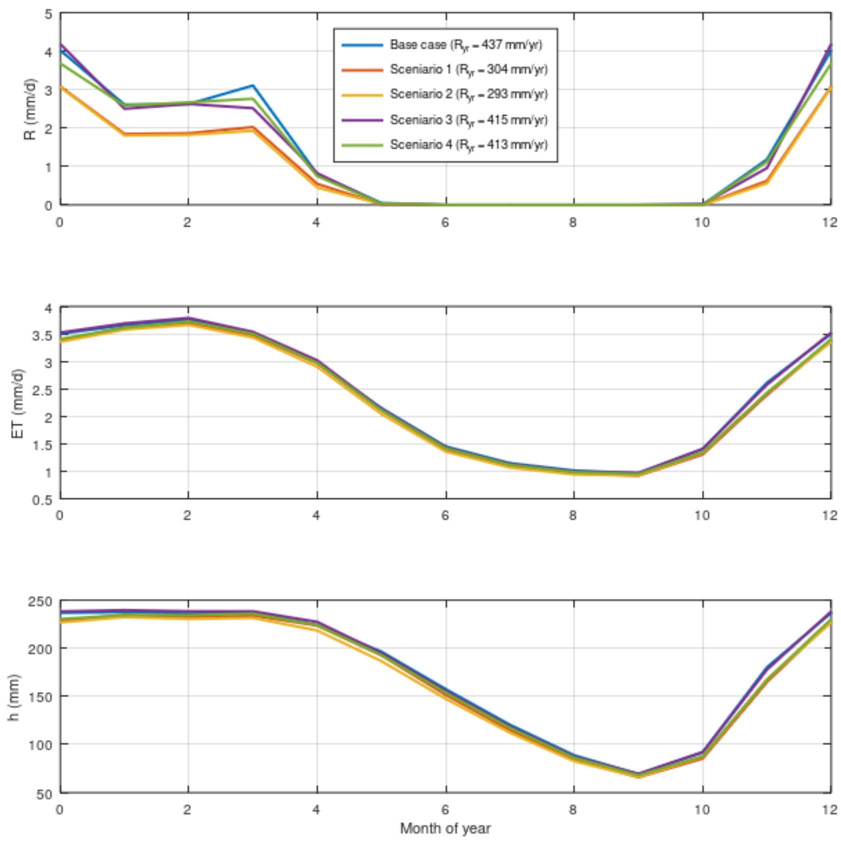

Figure S28. Same as Figure 10, but for Fazenda Planalto station.

MONTHLY MAPS OF PRECIPITATION *P*

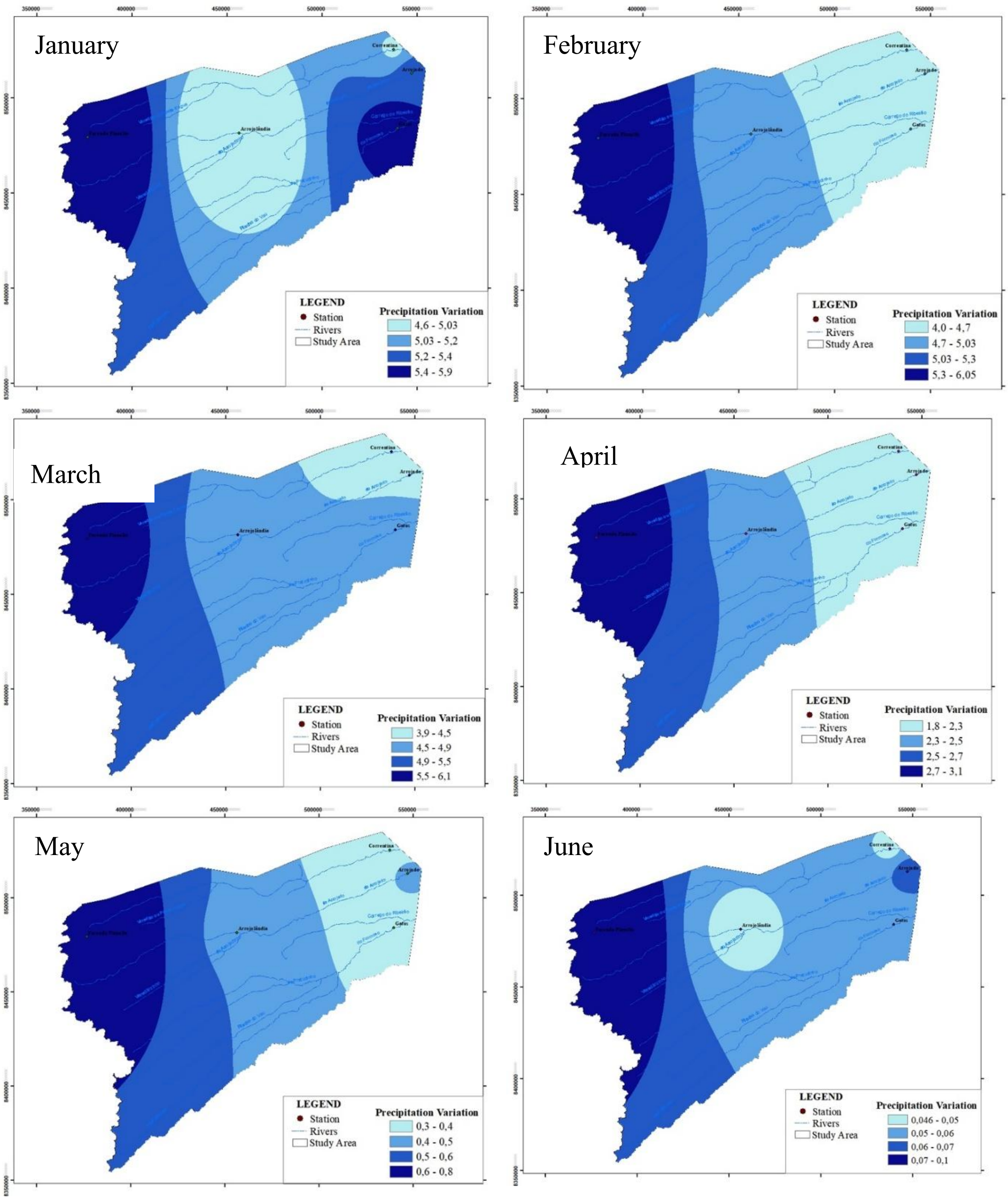

Figure S29. Monthly maps of precipitation *P* in mm/d.

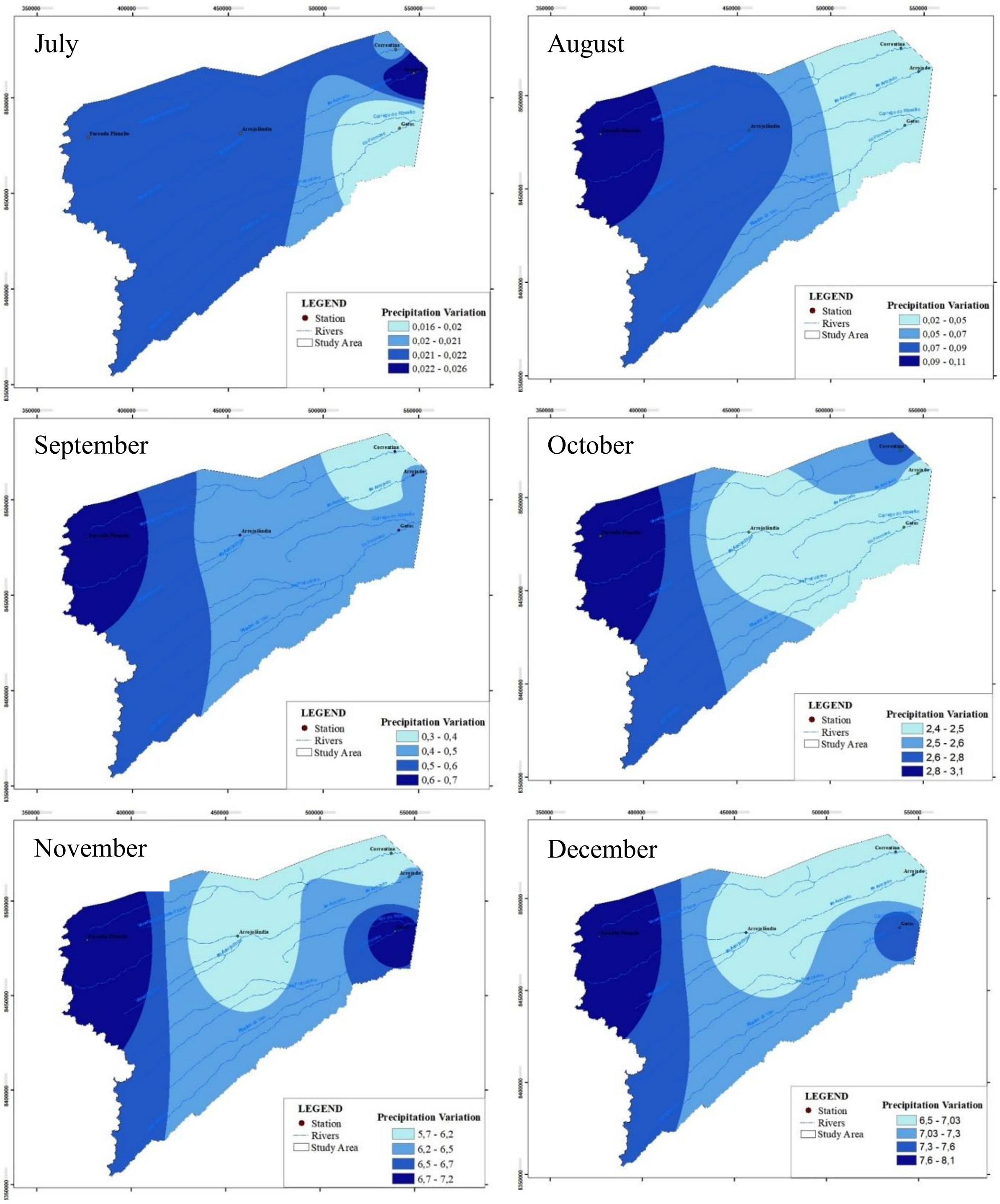

Figure S29 (continued). Monthly maps of precipitation *P* in mm/d.

MONTHY MAPS OF DAILY RAINFALL PROBABILITY λ

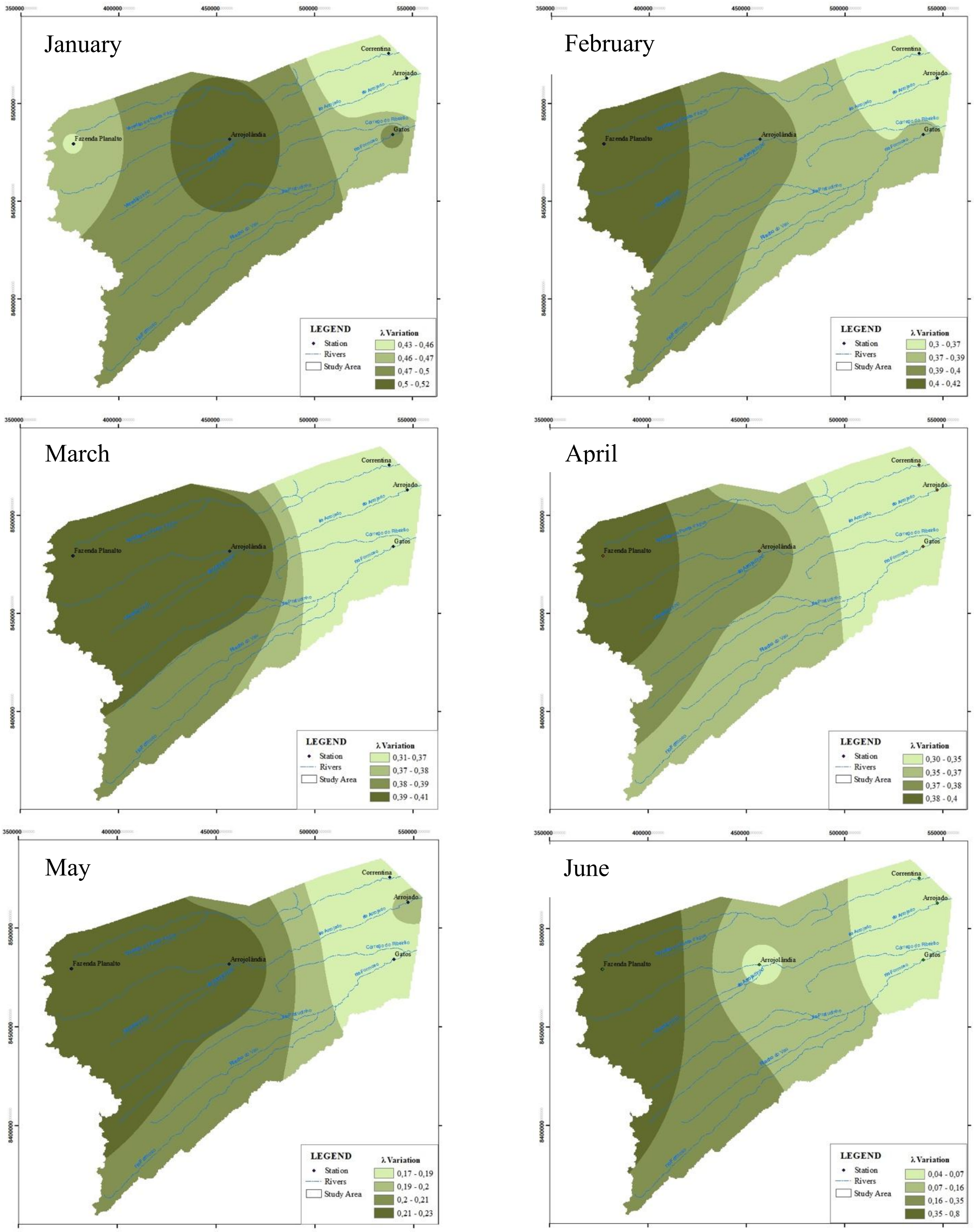

Figure S30. Monthly maps of daily rainfall probability λ in 1/d.

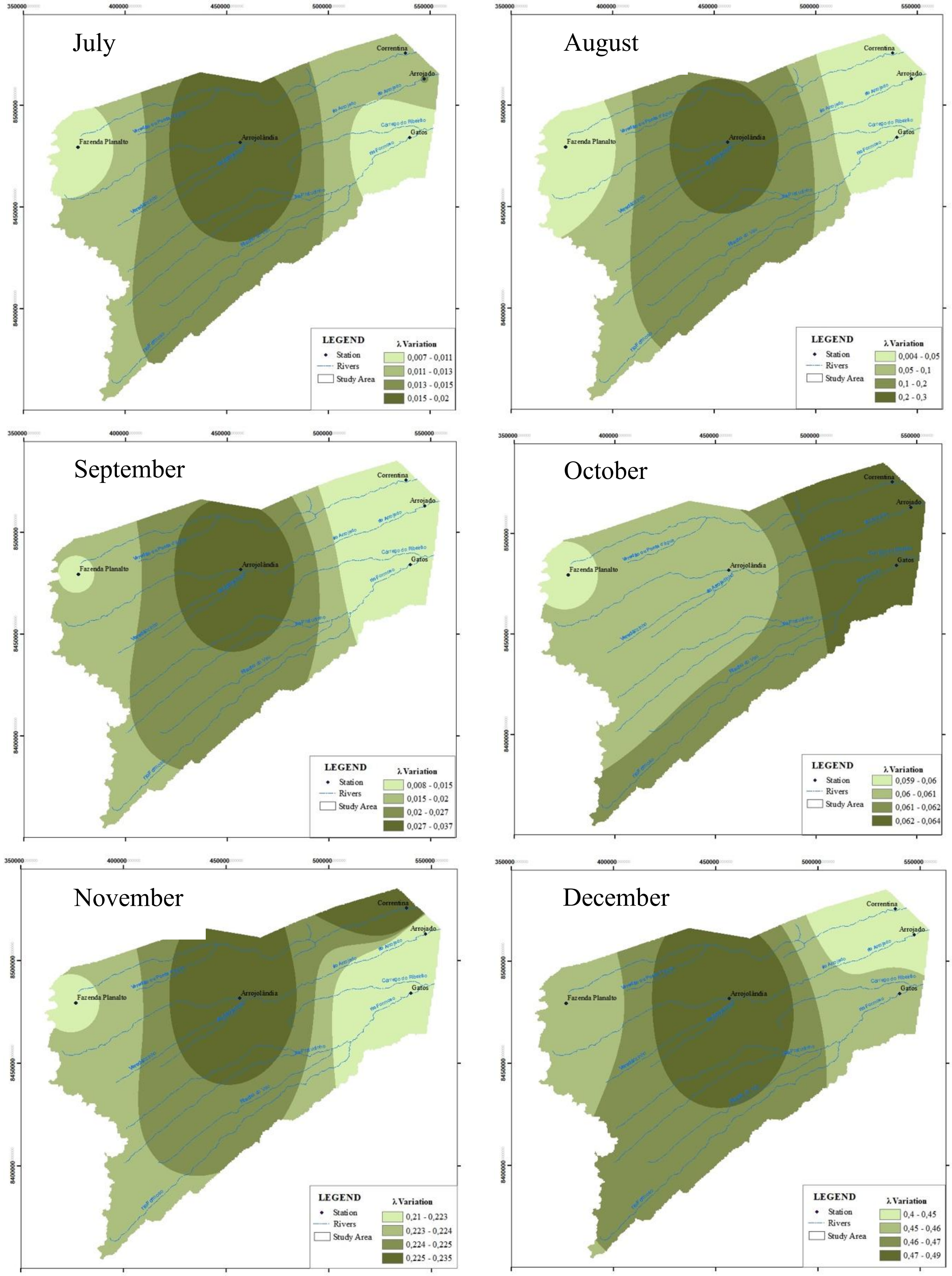

Figure S30 (continued). Monthly maps of daily rainfall probability λ in 1/d.

MONTHY MAPS OF AVERAGE RAINFALL INTENSITY ON RAINY DAYS α

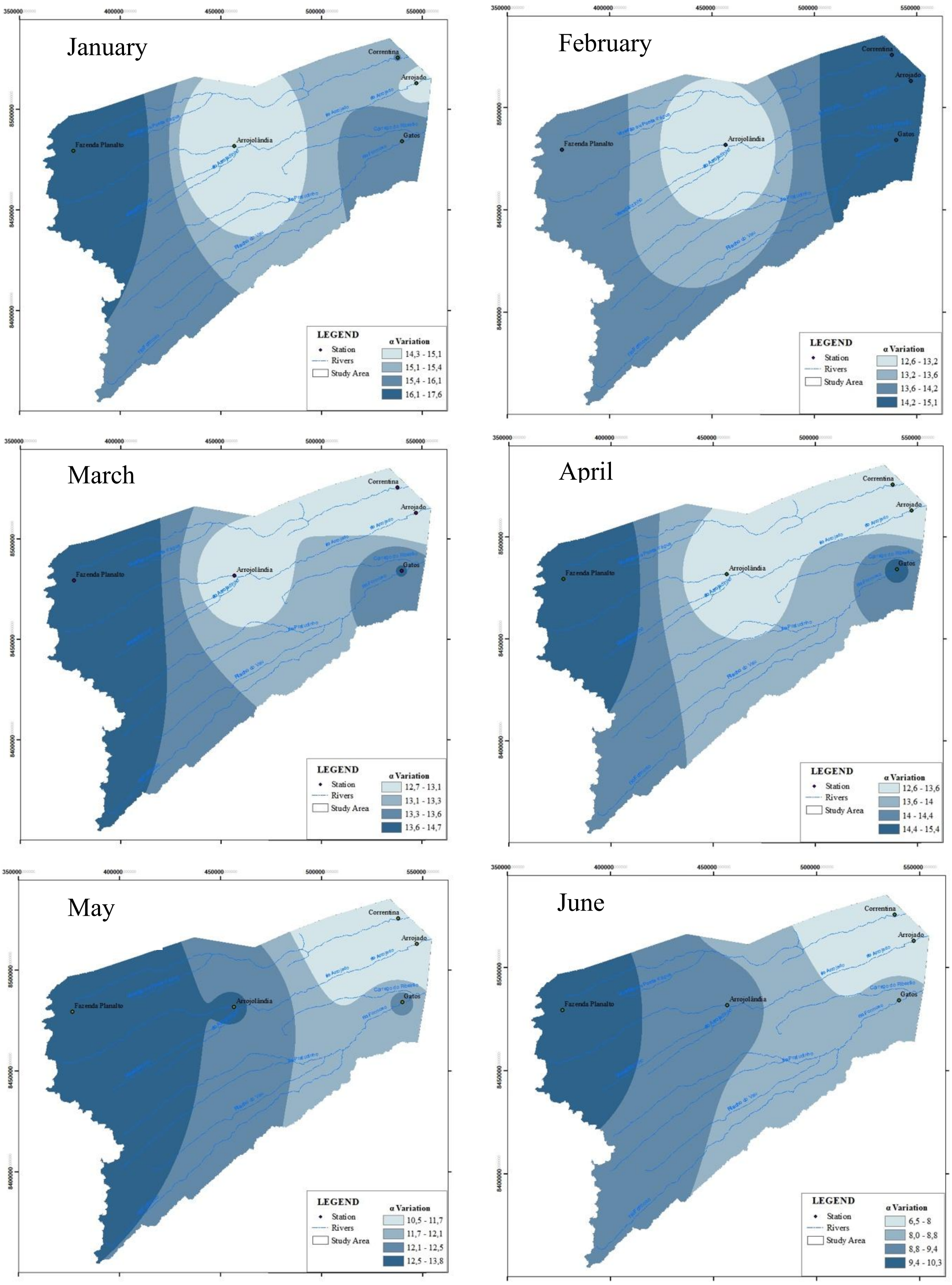

Figure S31. Monthly maps of average rainfall intensity on rainy days α in mm.

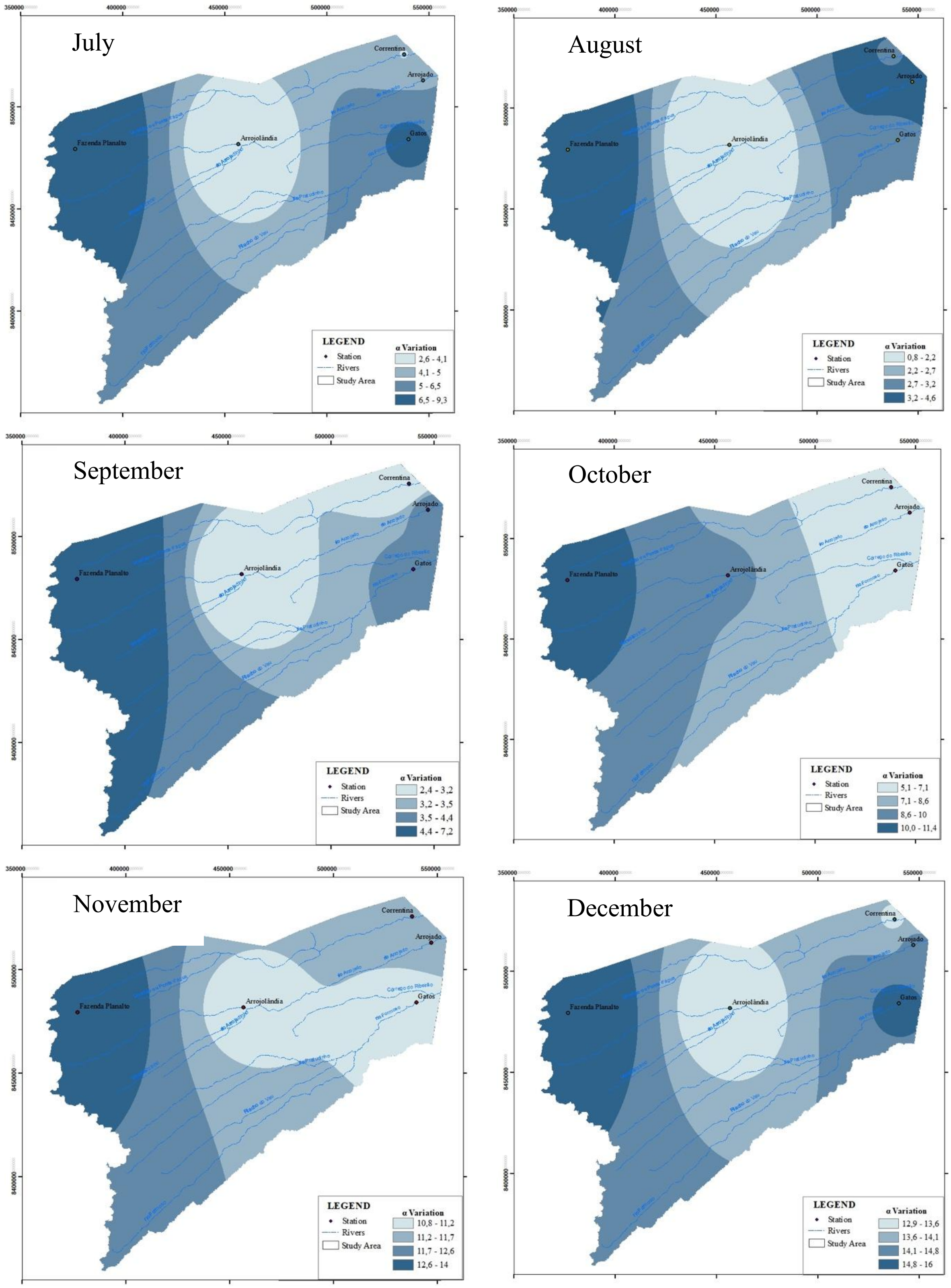

Figure S31 (continued). Monthly maps of average rainfall intensity on rainy days α in mm.

MONTHY MAPS OF ESTIMATED RECHARGE *R*

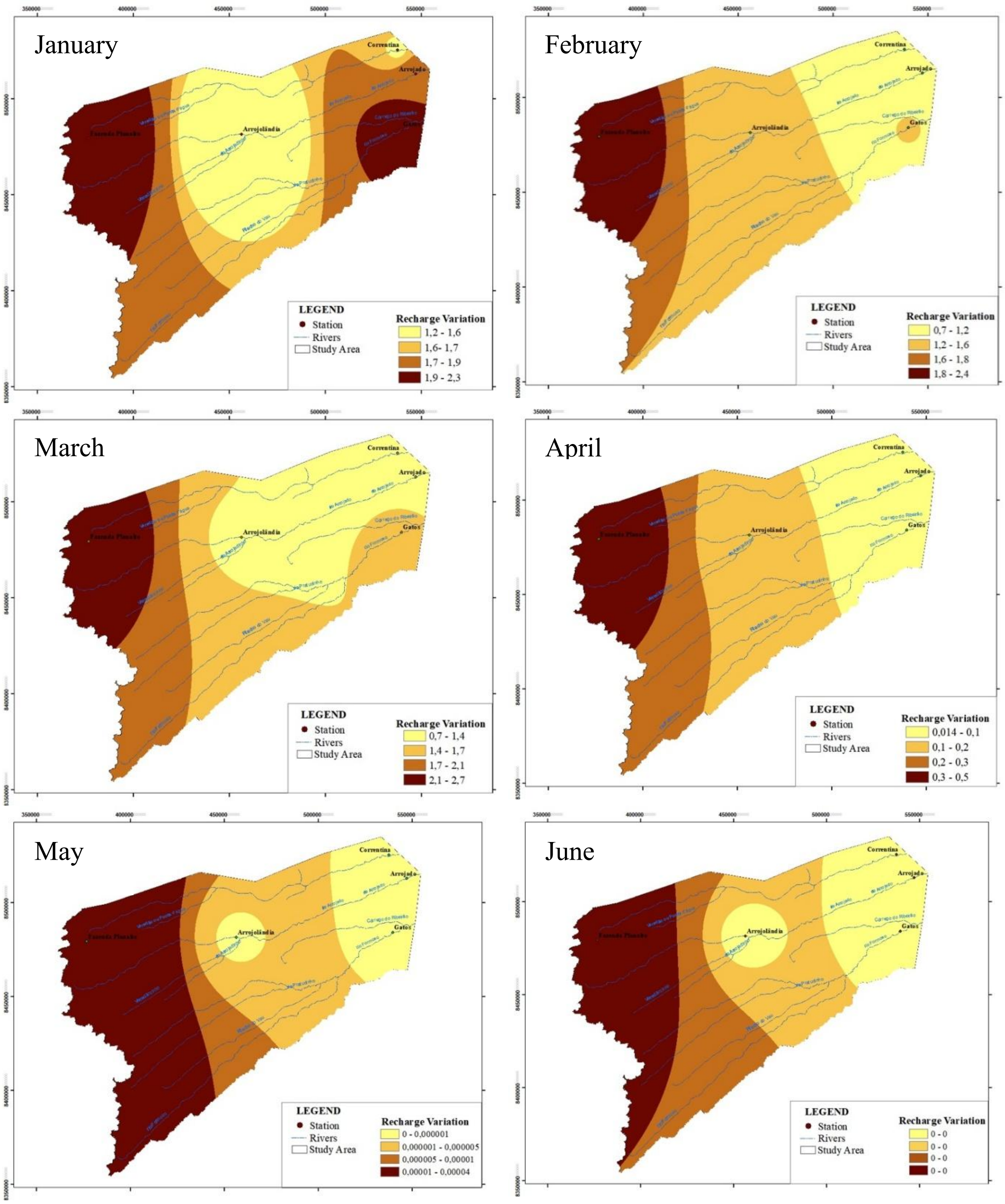

Figure S32. Monthly maps of estimated recharge *R* in mm/d.

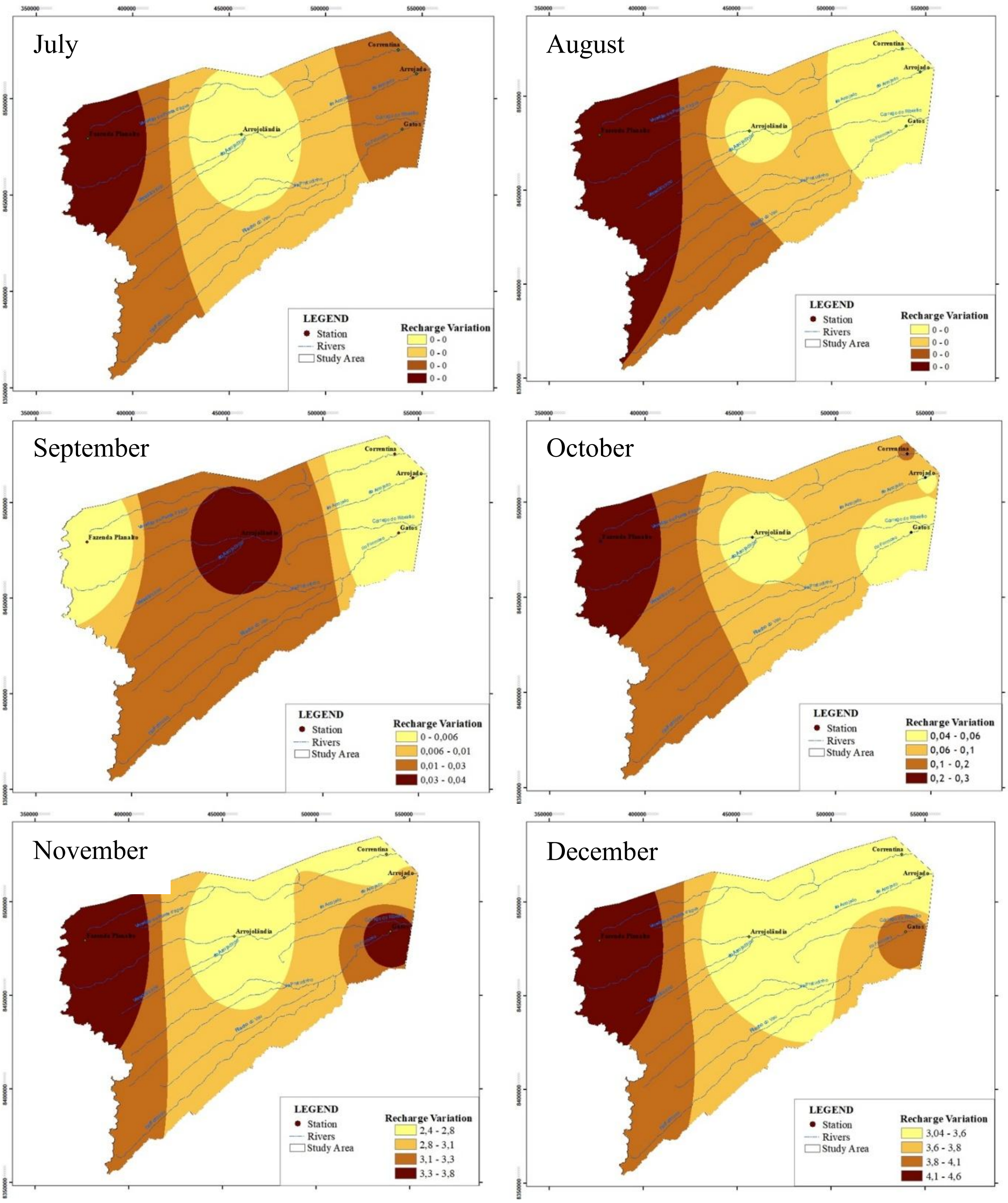

Figure S32 (continued). Monthly maps of estimated recharge *R* in mm/d.